

PREPARATION OF FUNCTIONALIZED GRAPHENES AND THEIR PERFORMANCE
FOR CORROSION RESISTANCE AND SYNTHESIS OF VANADIUM NITRIDE-
CARBON NANOFIBER MATS AND THEIR APPLICATION FOR ASYMMETRIC
SUPERCAPACITOR ELECTRODES

by

Melissa Ann Wunch

APPROVED BY SUPERVISORY COMMITTEE:

Duck Joo Yang, Chair

Kenneth J. Balkus, Jr.

John P. Ferraris

Ronald Smaldone

Copyright 2020

Melissa Ann Wunch

All Rights Reserved

I would like to dedicate this to my parents, whose endless love and support have kept me going.
And to my grandfather, who always reminded me to enjoy life and just keep going.

PREPARATION OF FUNCTIONALIZED GRAPHENES AND THEIR PERFORMANCE
FOR CORROSION RESISTANCE AND SYNTHESIS OF VANADIUM NITRIDE-
CARBON NANOFIBER MATS AND THEIR APPLICATION FOR ASYMMETRIC
SUPERCAPACITOR ELECTRODES

by

MELISSA ANN WUNCH, BS, MS

DISSERTATION

Presented to the Faculty of

The University of Texas at Dallas

in Partial Fulfillment

of the Requirements

for the Degree of

DOCTOR OF PHILOSOPHY IN

CHEMISTRY

THE UNIVERSITY OF TEXAS AT DALLAS

December 2020

ACKNOWLEDGMENTS

I would like to express my deepest appreciation to my advisor, Dr. DJ Yang, who has supported me throughout my journey at UT Dallas. I would also like to extend much appreciation to all of my committee members: Dr. Kenneth J. Balkus, Jr., Dr. John Ferraris, and Dr. Ronald Smaldone. Your guidance throughout this time has been invaluable.

A special thank you to all my friends at UT Dallas who have supported me throughout my PhD journey. Acknowledgement to Dr. Faisal Mahmood and Sangmin Lee for help with functionalization of graphene and corrosion performance. Thank you to all members in the Ferraris lab and Balkus lab for their support and input during my time at UT Dallas.

Appreciation to Bryan Salazar for all his help, input, and guidance in running and processing XPS spectra.

Finally, I would like to thank my parents and family for supporting me throughout all endeavors in my life. Your love and support were beyond measure and I will be forever grateful. I would also like to thank my loving and patient boyfriend, Alex, thank you for supporting and helping me for the last three years.

July 2020

PREPARATION OF FUNCTIONALIZED GRAPHENES AND THEIR PERFORMANCE
FOR CORROSION RESISTANCE AND SYNTHESIS OF VANADIUM NITRIDE-
CARBON NANOFIBER MATS AND THEIR APPLICATION FOR ASYMMETRIC
SUPERCAPACITOR ELECTRODES

Melissa Ann Wunch, PhD
The University of Texas at Dallas, 2020

Supervising Professor: Dr. Duck Joo Yang

Carbon materials have been researched in a wide range of applications, including energy storage, corrosion protection, catalyst support, etc. Though many people have studied properties of carbon with/without modification, research in the synthesis of functionalized carbon and carbon composites therefrom will be important. This dissertation outlines the synthesis of functionalized graphene, development of graphene composites, and metal nitride-carbon nanofiber composites and their application for electrode for super-capacitor.

Graphene is single layer carbon-based material known for its multifunctional properties (e.g. hydrophobicity, mechanical strength, etc.). This work studies application of graphene through functionalization of mechanically exfoliated graphene and functionalized graphene use for corrosion resistance. Functionalization of graphene is first discussed in the eco-friendly synthesis of aminated mechanically exfoliated graphene (MEG). Here we are able to directly functionalize MEG with amine groups using glycerol as the reaction medium and urea as the amine source.

The aminated MEG (AG) also showed enhanced dispersion stability in organic solvents and aqueous-solvent mixtures for >60 days. In the second area, we discussed how functionalized graphenes affected surface properties and corrosion resistance when composited with a polymer coating. Graphene, aminated graphene (AG), and fluorinated graphene (FG) were studied for corrosion resistance. Both AG and FG exhibited enhanced corrosion resistance when composited with a 2K urethane coating. Composite coating with FG showed a 94% increase in corrosion resistance versus graphene at a concentration of 4% by weight of solids. These materials also enhanced the surface properties of the coating. Electrochemical analysis of composite coatings showed that through inclusion of functionalized graphenes (AG or FG), barrier and adhesion properties were strengthened. Both FG and AG composite coatings showed an increase in contact angle versus graphene, with FG resulting in a hydrophobic surface (>90°) at 4wt%. This project shows a step towards the potential removal of sacrificial zinc as a barrier for corrosion resistance of steel substrate.

The increase in energy consumption over the last decade has led to research in the development of alternative energy storage devices which can meet the demand. Supercapacitors have garnered increased attention in this field due to their ability to provide high power and high energy. Electrodes within these devices can consist of two different materials, carbon or pseudocapacitive material. While carbon-based supercapacitors, or EDLCs, can provide high power density, they suffer from low energy densities. This has led researchers to study composite, or hybrid electrodes which combine the high power EDLC material with a high energy pseudocapacitive material (e.g. metal oxide or metal nitride). In the third area, we

assembled and tested hybrid-asymmetric devices using activated vanadium nitride-carbon nanofiber (VN-CNF) electrodes. The VN was made using vanadium oxide (V_2O_5) nanoflowers by a new synthesis method. Composite electrodes were made by electrospinning of a poly(acrylonitrile-co-itaconic acid) (PANIA) solution with the vanadium oxide (V_2O_5) nanoflowers dispersed within it to produce freestanding mats. VN-CNF freestanding mats were used as anode material and CNF as the cathode when assembling the device. Ionic liquid electrolyte 1-butyl-1-methylpyrrolidinium bis(trifluoromethanesulfonyl)imide ($Py_{14}TFSI$) with 0.5M lithium bis(trifluoromethanesulfonyl)imide ($LiTFSI$) was used, which widens the operating voltage window ($>3.5V$) compared with aqueous (e.g. KOH or Na_2SO_4) or organic electrolytes (e.g. $TEA-BF_4$ in ACN).

Chapter 1 introduces the material graphene, its properties, and methods of synthesis. In this section we also review methods of functionalization and application in the field of corrosion protection.

Chapter 2 describes the eco-friendly method of functionalization of mechanically exfoliated graphene (MEG) with amine groups and the effect of these groups on dispersion stability in organic solvents and aqueous-solvent mixtures are studied.

Chapter 3 studies the effect of graphene, aminated graphene (AG), and fluorinated graphene (FG) on surface properties and corrosion resistance when composited with a urethane coating. Contact angle measurements and electrochemical analysis were performed to determine which graphene and concentration provides best corrosion resistance.

Chapter 4 introduces supercapacitors and the concepts behind the different types. This section describes charge storage mechanisms of the pseudocapacitors and discusses different aspects of metal oxides and nitrides.

Chapter 5 describes the preparation of vanadium nitride-carbon nanofiber (VN-CNF) composite electrodes and analysis of their electrochemical properties. Charge contributions and storage mechanisms for each sample was studied to understand the mechanism in which their charge is stored (e.g. intercalative or pseudocapacitive/capacitive).

TABLE OF CONTENTS

ACKNOWLEDGMENTS	v
ABSTRACT.....	vii
LIST OF FIGURES	xiv
LIST OF TABLES	xvii
CHAPTER 1 INTRODUCTION: SYNTHESIS AND APPLICATIONS OF FUNCTIONALIZED GRAPHENE.....	2
CHAPTER 2 GREEN SYNTHESIS OF AMINATED MECHANICALLY EXFOLIATED GRAPHENE	9
Abstract.....	10
2.1 Introduction.....	10
2.2 Experimental.....	12
2.3 Results and Discussion	13
2.4 Conclusion	22
CHAPTER 3 AMINATED AND FLUORINATED GRAPHENE BASED COATING FOR CORROSION RESISTANCE	23
Abstract.....	24
3.1 Introduction.....	24
3.2 Experimental.....	27
3.3 Characterization.....	29
3.3 Results and Discussion	30
3.4 Conclusion	36
II. SYNTHESIS OF VANADIUM NITRIDE-CARBON NANOFIBER MATS AND THEIR APPLICATION FOR ASYMMETRIC SUPERCAPACITOR ELECTRODES	37
CHAPTER 4 INTRODUCTION	38
CHAPTER 5 VANADIUM NITRIDE-CARBON NANOFIBER (VN-CNF) COMPOSITE ELECTRODES FOR ASYMMETRIC SUPERCAPACITORS	46
5.1 Introduction.....	46
5.2 Experimental.....	49
5.3 Results and Discussion	52

5.4 Conclusion	63
5.5 Appendix: Supplemental.....	65
REFERENCES	67
BIOGRAPHICAL SKETCH	78
CURRICULUM VITAE	

LIST OF FIGURES

Figure 1.1 Structure of Graphene.....	2
Figure 1.2 Structure of Graphene Oxide.....	4
Figure 2.1 Proposed reaction mechanism for amine functionalization of MEG with urea	14
Figure 2.2 FTIR spectra of (a) MEG and (b) AG	15
Figure 2.3 XPS spectra of (a) the C1s of MEG and (b) the C1s and (c) N1s of sputtered AG	16
Figure 2.4 Raman spectra of (a) MEG and (b) AG.....	17
Figure 2.5 XRD pattern of (a) MEG and (b) AG.....	18
Figure 2.6 TGA analysis of (a) MEG and (b) AG	19
Figure 2.7 AG dispersions at Day 0 (top) and Day 60 (bottom).....	20
Figure 2.8 AG dispersions in Ethylene glycol:DI-H ₂ O mixtures at Day 0 (top) and Day 60 (bottom).....	21
Figure 3.1 Characterization of functionalized graphenes. (a) FTIR, (b) Raman spectra showing characteristic D and G bands, and (c) TGA of G, AG, and FG	30
Figure 3.2 Contact angle measurements of G, AG, and FG in 2K Urethane coating as a function of increasing graphene content	32
Figure 3.3 Corrosion results of (a) 0%, (b-d) 1, 2, and 4wt% AG, and (e-g) 1, 2, and 4wt% FG	33
Figure 3.4 Corrosion rate comparison: 0% vs. G vs. AG vs. FG.....	34
Figure 3.5 Impedance data from EIS analysis of 4% G, 4% AG, and 4% FG coated substrates .	35
Figure 4.1 Ragone Plot	39
Figure 4.2 Pictorial representation of the charge storage mechanism for each category of supercapacitor. (a) EDLC, (b) intercalative pseudocapacitor, and (c) hybrid	40
Figure 4.3 Structure of ionic liquid electrolytes commonly used in supercapacitors.....	45

Figure 5.1 XRD patterns of activated (a) CNF, (b) 15VN-CNF, (c) 30VN-CNF, and (d) 45VN-CNF.....	53
Figure 5.2 SEM images of activated (a) CNF, (b) 15VN-CNF, (c) 30VN-CNF, and (d) 45VN-CNF.....	54
Figure 5.3 TEM imaging of (a) CNF, (b) 15VN-CNF, (c) 30VN-CNF, and (d) 45VN-CNF.....	55
Figure 5.4 XPS spectra of (a) C1s, (b) O1s, and (c) N1s for activated CNF and (d) C1s, (e) V2p, (f) N1s for activated 45VN-CNF	56
Figure 5.5 Raman spectra of (a) CNF, (b) 15VN-CNF, (c) 30VN-CNF, and (d) 45VN-CNF.....	58
Figure 5.6 Pore size distribution of activated CNF and VN-CNF composites.....	58
Figure 5.7 Cyclic Voltammetry (CV) results for (a) CNF, (b) 15VN-CNF, (c) 30VN-CNF, and (d) 45VN-CNF	60
Figure 5.8 (a) CDC curves of CNF and VN-CNF composites, (b) Ragone Plot, and (c) Cycle test of 45VN-CNF after 8000 cycles.....	60
Figure 5.9 Separation of charge contribution for (a) 15VN-CNF, (b) 30VN-CNF, (c) 45VN-CNF, and (d) <i>b</i> values for VN-CNF composites	62
Figure 5.10 XRD of (a) as-synthesized V ₂ O ₅ nanoflowers and (b) V ₂ O ₅ nanoflowers annealed at 900°C for 2h under N ₂	65
Figure 5.11 (a) SEM V ₂ O ₅ nanoflowers and TEM imaging of (b) as-synthesized nanoflowers and (c) probe sonicated nanoflowers	65
Figure 5.12 XPS of V ₂ O ₅ nanoflowers	66

LIST OF TABLES

Table 1.1 Summary of the common methods used for fluorinated graphene synthesis	6
Table 5.1 I_D/I_G ratios and conductivities of activated CNF and VN-CNF composites.....	57
Table 5.2 BET surface area of activated CNF and VN-CNF composites	59
Table 5.3 Electrochemical performance of VN-CNF hybrid-asymmetric devices.....	59

**I. PREPARATION OF FUNCTIONALIZED GRAPHENES AND THE PERFORMANCE
FOR CORROSION RESISTANCE**

CHAPTER 1
INTRODUCTION: SYNTHESIS AND APPLICATIONS OF
FUNCTIONALIZED GRAPHENE

1.1 Introduction

Graphene and its methods of production

Graphene is a single layer, carbon-based material with sp^2 hybridized carbons arranged in a hexagonal lattice structure¹. Figure 1.1 displays the basic structure of graphene with sp^2 hybridized carbon structure.

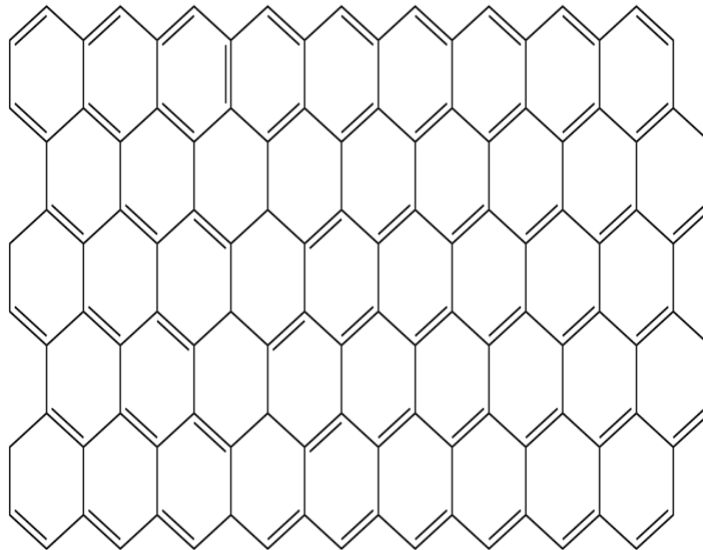


Figure 1.1. Basic structure of Graphene with C=C

Due to its multifunctional properties it has been researched for a wide range of applications. These properties include high mechanical strength (Modulus: 1000 GPa and Strength: 5 GPa), barrier property, hydrophobicity, surface area ($2600 \text{ m}^2/\text{g}$), electronic conductivity (10^7 S/m), etc¹. Because of these properties, graphene has been studied as an additive in resins for corrosion resistance or as a material for energy storage devices (e.g. supercapacitors or Li-ion batteries)²⁻³. Single layer graphene has been synthesized using various methods, including chemical vapor

deposition (CVD), mechanical exfoliation, chemical exfoliation, etc². CVD synthesis of graphene can be broken down into two categories: plasma and thermal³⁻⁵. Thermal CVD method of synthesis is considered to be the most cost-effective method of production⁶. However, this process requires high temperatures and metallic substrates for carbon growth, which can be difficult to remove. The method of plasma CVD offers a means to produce graphene with lower temperature and an insulative substrate, eliminating the difficulty of removing the metallic substrate used during thermal CVD^{4, 7}. While these methods can produce single layer graphene, it has still proven to be difficult to produce at the bulk scale. Both methods are currently used primarily for graphene film production. Production of single or few-layered graphene at a larger scale has been achieved by mechanical exfoliation of graphite⁸⁻¹¹. Mechanical exfoliation can be performed using different methods, the most common being ball milling¹¹. The method of scotch tape mechanical exfoliation is known as micromechanical exfoliation, which requires several applications of the normal force in order to finally obtain a single layered graphene structure¹²⁻¹³. The Nobel Prize in 2010 was awarded for discovering the first monolayer structure of graphene obtained using the scotch tape method¹³. Ball milling uses shear force to produce graphene with multiple layers, which can be as small as 100 nm in diameter^{11, 14-15}. During the process of ball milling the high degree of shear force generated leads to exfoliation and cracking of C-C bonds¹⁴. There are different angles in which the force can collide with the graphite during the milling. This produces reactive carbon species, typically along the edges of the graphene, allowing for functionalization or doping to occur without treatment with caustic oxidizing agents¹⁵⁻¹⁷.

Functionalization of Graphene

Graphene has been functionalized with a number of different groups on its surface. These include amine, carboxyl, hydroxyl, epoxy, or heteroatoms¹⁷⁻¹⁹. Heteroatom functionalization introduces sulfur, fluoride, or boron groups either along the edge or in the basal plane of the graphene^{18, 20}. The methods in which these functional groups introduced on the surface or along the edges has a degree of variation¹⁴⁻¹⁵.

Surface functionalization of graphene with carboxyl, hydroxyl, and epoxy groups produces what is known as graphene oxide or GO. Synthesis of GO is often performed through the Modified Hummer's method²¹⁻²³. This method treats a graphitic precursor (e.g. graphite or exfoliated graphene) with a series of strong oxidizers, such as concentrated sulfuric acid (H₂SO₄), potassium permanganate (KMnO₄), and sodium nitrate (NaNO₃). The structure of GO is displayed in Figure 1.2.

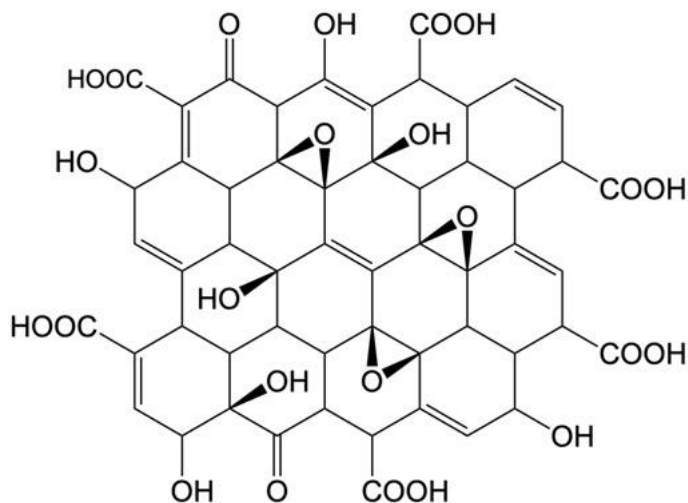


Figure 1.2. Structure of Graphene Oxide

While this method is the most widely used, many have established methods to reduce or eliminate the amount of noxious gases which are released (e.g. NO or NO_x). Wang *et al.*

developed a method of GO synthesis which eliminates the use of NaNO_3 during synthesis by using a mixture of H_2SO_4 and H_3PO_4 ²⁴. An environmentally friendly method for GO production has also been reported which eliminates the use of any oxidizing agents²⁵. This approach follows a bottom-up synthesis through the polymerization glucose²⁵. Glucose solution was treated hydrothermally to produce sheets of GO²⁵. Graphene oxide can also be used as a precursor material for the production of other functionalized graphene products, such as aminated graphene or fluorinated graphene²⁶⁻²⁹. While GO can enhance some properties of graphene, introduction of amine or fluorine groups on the surface can provide additional benefits for strength, thermal conductivity, electrical conductivity, etc^{18, 20, 30-31}.

Amine functionalized graphene is synthesized by treating GO with an amine precursor³⁰⁻³⁵. This precursor can be ethylenediamine (EDA), *para*-phenylenediamine (PPDA), trimethylamine (TEA), urea, etc³³⁻³⁵. These methods either disperse the GO in a solution of the amine source for 24-48h or treat the GO-amine dispersion hydrothermally to produce the aminated GO (AGO) material. Ram *et al.* treated GO with PPDA to synthesize AGO. They studied the effect of amine groups on corrosion protection when used as an additive in an epoxy-based coating³⁴. Amine functional groups can also help enhance the strength of materials such as epoxy resins or urethane resins. This is due to the ability of the $-\text{NH}_2$ groups to form covalent bonds with the resin, helping to increase strength and durability. In these studies, alkylated amines with varying chain lengths are used for functionalization on the surface³⁶.

Fluorination of graphene has been performed through a wide range of synthetic methods¹⁸. Table 1.1 outlines a few of the common methods and graphitic precursors used for fluorination.

Table 1.1. Summary of the common methods used for fluorinated graphene synthesis

	Method		Temperature	Time
	Graphene	Fluorine Agent/Exfoliation Solvent		
Direct Gas	Graphene, GO, Graphite	XeF ₂ , F ₂	30-600°C	20 min to 2 weeks
Exfoliation	Fluorinated Graphite	H ₂ SO ₄ /H ₃ PO ₄ , NMP, ACN	25-50°C	10 min to 100h
Plasma	CVD Graphene, GO	CF ₂ , SF ₆	25-200°C	6s to 30h
Hydrothermal	Graphene Oxide (GO)	HF, DAST	50-180°C	17 to 24h

*DAST: Diethylaminosulfur trifluoride, NMP: N-Methyl-2-pyrrolidone, ACN: Acetonitrile

One method of fluorination is direct gas fluorination. This treats the graphitic material (e.g. GO, Graphite, HOPG, etc.) with a fluorine gas source such as F₂ or XeF₂^{18, 37-38}. Through tuning of synthesis conditions, such as temperature and/or time, researchers have been able to adjust the fluorine content present in the material^{18, 20, 38}. FGO can also be synthesized by the chemical exfoliation of fluorinated graphite, or fluorographene^{20, 39}. In this method the fluorographene is sonicated in an organic solvent (e.g. NMP) then collected by either vacuum filtration or centrifugation¹⁸. Synthesis of FGO by treatment GO with F₂ or XeF₂ is also known as direct gas fluorination. This method of fluorination is typically performed in a pressurized reactor in which the fluorine gas is introduced. Concentration of fluorine used during synthesis can be as high as 20% F₂ or as low as 5% F₂ in the mixture. Mazanek *et al.* fluorinated GO using a 20% F₂/N₂ gas mixture under hydrothermal conditions³⁸. The fluorine content in the samples were adjusted by changing either the time of fluorination or temperature³⁸. This study displayed that with increasing temperature the fluorine content present on the surface increased by approximately 30% and by subsequently increasing time, it was increased by 50%. As stated previously, FG can also be synthesized by the chemical exfoliation of fluorographene. Fluorinated graphite, or

fluorographene, is a graphitic material consisting of sp^3 hybridized carbons to which a fluorine is bound to each carbon^{20, 40}. While this material has a high degree of thermal stability, it is also insulating and highly reactive²⁰. In order to produce single layered FG from this material, several groups have used what is known as chemical exfoliation. This is where the multi-layered fluorographene is dispersed in an organic solvent by means of either bath sonication or probe sonication⁴¹. Solvents often used during this process are either NMP or DMF¹⁸. Due to the high thermal stability and degree of hydrophobicity the fluoride groups offer, FG there has been used in a variety of applications. Mathkar *et al.* reported the application of FG for the use in self-cleaning inks³⁹. Their group synthesized a highly fluorinated graphene oxide (HFGO) which displayed amphiphobic property upon being coated onto a silicon wafer³⁹.

Graphene for Corrosion Protection

The high surface area, barrier and hydrophobicity properties of graphene have led to increased research for its application in the field of corrosion protection⁴². Graphene's high barrier, high hydrophobicity and high surface area have shown that it can be a promising additive material for coatings. Surface functionalization of graphene can help to enhance the properties of graphene, i.e. barrier, hydrophobicity, electrical and thermal conductivities, etc^{18, 43-44}. The functional groups on graphene can also help to prevent the re-stacking observed when using pristine graphene⁴⁵⁻⁴⁶.

Functionalized graphene for corrosion protection has been composited primarily in epoxy-based coatings. Amine functionalized graphene can react with the epoxy groups present in the coating forming covalent bonds. This can help enhance the strength of the coating and barrier protection^{34, 36, 44}. Fluorinated graphene helps to enhance the surface properties of the coatings

due to the high degree of electronegativity of the fluoride groups^{40, 47}. When composited with a coating the fluoride groups help to further enhance its hydrophobicity compared to graphene. The increase in hydrophobicity as well as high surface area of graphene (2,630 m²/g) allow for the water, ions or other molecules to wick away allowing for further difficult to penetrate the coating to reach at the surface of metal substrate ^{40, 47}.

CHAPTER 2

GREEN SYNTHESIS OF AMINATED MECHANICALLY EXFOLIATED GRAPHENE¹

Authors- Melissa A. Wunch^a, Bryan G. Salazaar^a, and Duck Joo Yang^{a*}

^aDepartment of Chemistry and Biochemistry, BE26

The University of Texas at Dallas

800 West Campbell Road

Richardson, Texas 75080-3021

¹Manuscript Title: “Green Synthesis of Aminated Mechanically Exfoliated Graphene” under correction to *RSC Advances*

Abstract

Graphene based materials have shown promise in a wide range of applications. We report an eco-friendly method for the amination of mechanically exfoliated graphene. Mechanically exfoliated graphene eliminates the use of concentrated acids and strong oxidizers or reducing agents used during pre-functionalization, in addition to eliminating the use of caustic and light sensitive amine precursors. Use of urea as the amine source, glycerol as the solvent, and synthesis at 1 atm, decreases the cost and environmental impact of this method. Chemical and physical characterization of synthesized aminated graphene (AG) was determined by FTIR, XPS, Raman, and XRD. Thermal stability of the AG was determined by thermal gravimetric analysis (TGA). FTIR spectral analysis identified the presence of N-H and C-N vibrational modes. While XPS showed the binding energies corresponding to NH₂-C and N-C bonding. Dispersion studies showed that in a system with ethylene glycol and water, AG maintained stability for longer than 60 days. This dispersion mixture presents a less caustic solvent system to generate stable dispersions.

2.1 Introduction

Graphene is a single layered carbon-based material with sp² hybridized carbons arranged in a hexagonal lattice.^{1, 19, 21, 48-49} Due to its multifunctional properties, it has been used in a wide variety of applications such as electronics, composite coating, corrosion protection, and energy storage.^{45, 49-52} These multifunctional properties include high surface area, hydrophobicity, barrier properties, and enhanced mechanical strength.^{1, 18, 48-49, 53-54} Taking advantage of the high surface area, hydrophobic, and barrier property of graphene have led to its application as an additive in polymer coatings for corrosion protection.^{48, 50, 54-56} To enhance these properties, functional groups have

been introduced on the surface.^{28, 34, 47, 57-59} These functional groups help to enhance dispersion and surface properties of graphene.^{28, 58-60} Functional groups which are commonly introduced on the surface include: carboxyl, hydroxyl, epoxy, fluoride, and amine.^{18-19, 30, 61-62}

Aminated graphene oxide (AGO) has been synthesized by the treatment of graphene oxide (GO) with various amine sources^{28, 30, 32, 35, 63-64}. Precursor GO is synthesized by treatment of graphite with a series of strong oxidizers (e.g. sulfuric acid, sodium nitrate, potassium permanganate, and hydrogen peroxide). This introduces oxygen functionalities on the surface, such as carboxyl (-COOH), hydroxyl (-OH), and epoxy²¹⁻²³. Treatment of GO with amine precursors (e.g. para-phenylenediamine, ethylenediamine, trimethylamine, ammonia, urea, etc.) produced AGO^{28, 30, 32, 34-35}. Synthesis reported by Tetsuka *et al* reported amination of GO using an aqueous urea solution to produce AGO.⁶⁵ This synthesis was performed in an autoclave, which can limit the scalability of the synthesis⁶⁵. Our new method outlined in this paper is, to the best of our knowledge, the first to directly amination of mechanically exfoliated graphene (MEG) with urea using glycerol or glycol reaction medium at ambient pressure. Preparation of MEG does not require caustic oxidizers, thus eliminating generation of hazardous waste.

Furthermore, the direct amination of MEG eliminates the use of highly corrosive chemicals, reduction of GO, and expensive aminating compounds (i.e. strong oxidants/acids, hydrazine, ethylenediamine, trimethylamine, etc.). This method employs urea as the source for amination and glycerol as the solvent system for synthesis. These materials help to decrease the overall environmental impact. The high boiling point of glycerol (290°C) allows the reaction to be performed under ambient pressure (1atm), thus eliminating the use of an autoclave. It will therefore reduce capital investment for scale-up production. We also found no need of catalysts

in order to aid in the reaction can lead to potential recycling of the reaction media. This decreases the quantity of waste generation leading to a more environmentally benign and economical synthesis method.

2.2 Experimental

Materials

Mechanically exfoliated graphene (C-Grade, 99% Carbon) was purchased from XG Sciences. Acetone (Reagent Grade), Glycerol (Certified ACS Grade), Isopropanol (IPA, Certified ACS), and N,N-Dimethylformamide (DMF, 99.5%, Certified ACS) were purchased from Fisher Chemical. N-Methyl-2-pyrrolidone (NMP, Spectroscopy Grade, 99.9%), Ethanol (190 Proof), and Xylenes (Reagent Grade, 98%) were purchased from Alfa-Aesar. Urea (ACS Grade, 99%) was purchased from Sigma-Aldrich. All chemicals were used as purchased without any further purification.

Synthesis of Aminated Graphene (AG)

Mechanically exfoliated graphene (1.0 g, C-Grade, >99% Carbon) was dispersed in Glycerol (100mL) for 30 minutes by magnetic stirring in a 250mL round bottom flask. Urea (1.0 g) was then added to the dispersion at a 1:1 weight ratio with respect to graphene. The dispersion was heated up to 190°C and refluxed for 5h. After reaction completion, the graphene was vacuum filtered and dried under vacuum at 225°C for 24h in order to eliminate any residual solvent that may be trapped in the sample. The dried sample was then collected and used for characterization.

AG Solvent Dispersions

Aminated graphene dispersions were prepared by probe sonication for 3, 30 second intervals. The samples were placed in an ice bath in between each sonication. AG at a concentration of 0.1mg mL⁻¹ was dispersed in various organic solvents. After sonication, the samples were then monitored

over time in order to observe the stability of these dispersions. Dispersions consisting of ethylene glycol and water followed the same sonication procedure as outlined above. The concentration of AG was also maintained at 0.1mg mL^{-1} for those dispersions in order to maintain consistency throughout all experiments.

Characterization

Physical characterization of AG was performed using FTIR, Raman, and powder X-ray Diffraction (XRD) methods. FTIR was performed using a KBr pellet on a Nicolet Avatar 360 FTIR with a range of $400\text{-}4000\text{ cm}^{-1}$. Raman characterization was performed using a Jobin Yvon LabRam HR Micro-Raman spectrometer with a He-Ne laser source at a wavelength of 633 nm. Powder X-ray diffraction (XRD) on all graphene samples was performed using a Rigaku Ultima IV with Cu-K α as the X-ray source. Chemical composition of the AG was performed by X-ray photoelectron spectroscopy (XPS) through determination of binding energies of the functionalized graphene. XPS was performed *ex situ* using a PHI VersaProbe II Scanning XPS Microprobe with an Al-K α (1486.6eV) X-ray source. Spectra were collected using a 23.5eV pass energy and a 0.1eV step energy. No charge compensation was used. Sample surface was sputtered using Ar gas ion cluster beam to measure nitrogen under the surface. Thermal analysis of AG was performed using a TA Q600 SDT simultaneous TGA/DSC with a temperature range of $25\text{-}800^\circ\text{C}$ at a ramp rate of 5°C min^{-1} while under continuous nitrogen (N $_2$) flow.

2.3 Results and Discussion

Amination of graphene was performed by a facile reflux method using mechanically exfoliated graphene (MEG) nanoplatelets, urea, and glycerol. Exfoliation of graphene by mechanical methods (e.g. ball milling) can lead to the production of surface defects, cracking of C=C bonds,

leading to the formation of carbon radicals along the edges^{14-15, 17, 66}. Through this means of exfoliation it is possible to form more reactive carbon centers along the edges of the graphene^{17, 66}. This increases the chemical reactivity of graphene, primarily along the edges, and leads to the ability to directly react functional groups with the material. Formation of these electroactive centers allow for more nucleophilic reactants to interact with the graphene for functionalization. Scheme 1 outlines the proposed mechanism for the functionalization of the graphene nanoplatelets using urea. At high temperature ($>150^{\circ}\text{C}$) urea decomposes to form ammonia ($\text{NH}_3(\text{g})$) gas. The ammonia gas reacts with the carbon radical centers on the graphene to produce $-\text{NH}_3^+$ groups. A proton can then be abstracted to form the final $-\text{NH}_2$ functional groups present on the graphene edges.

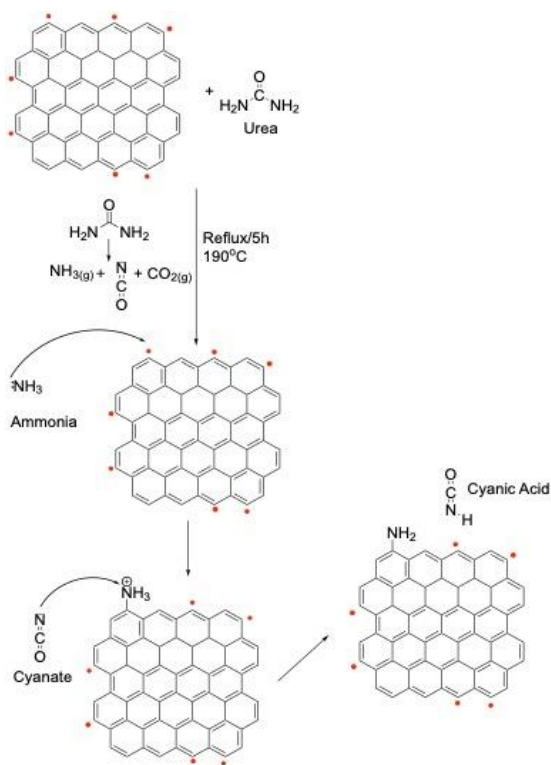


Figure 2.1. Proposed reaction Mechanism for the amine functionalization of MEG with urea.

Amination of mechanically exfoliated graphene was performed through reflux of urea and graphene in glycerol. Urea serves as a greener alternative amine source for functionalization. Presence of amine groups on the surface was confirmed by FTIR analysis on the material. Spectra of MEG and AG synthesized in pure glycerol are shown in Figure 2.2. Vibrational bands at 3500-3650 and 1573 cm^{-1} in the AG sample corresponds to N-H stretching and bending modes, respectively. A vibrational band at 1103 cm^{-1} was observed in the spectra corresponding to the aromatic C-N bonding. In the IR spectra for pristine graphene only the vibrational modes observed in the fingerprint region, C=C and =C-H, are observed. There is no presence of N-H or C-N modes.

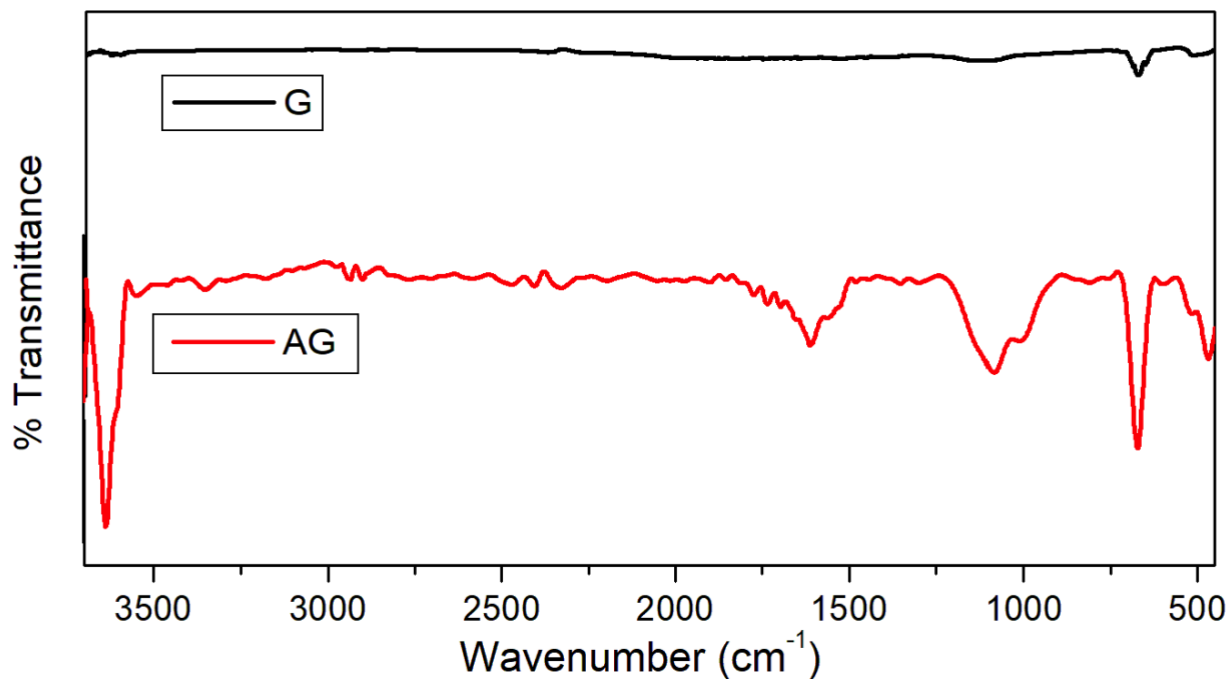


Figure 2.2. FTIR Spectral Analysis of a) MEG and b) AG

XPS analysis was performed on the functionalized material in order to identify the chemical composition and binding energies of the amine groups. After curve fitting of the C1s spectra, the sp^2 -C peak at 284.3eV was observed in addition to the π - π^* satellite peak in both MEG and AG

(Figure 2.3a and 2.3b). Peaks observed at 400.6eV and 399.0eV in the N1s spectra, were representative of the H₂N-C and N-C= moieties, respectively (Figure 2.3c). The XPS data presented is post-sputtering and confirms the presence of –NH₂ groups on the functionalized graphene samples.

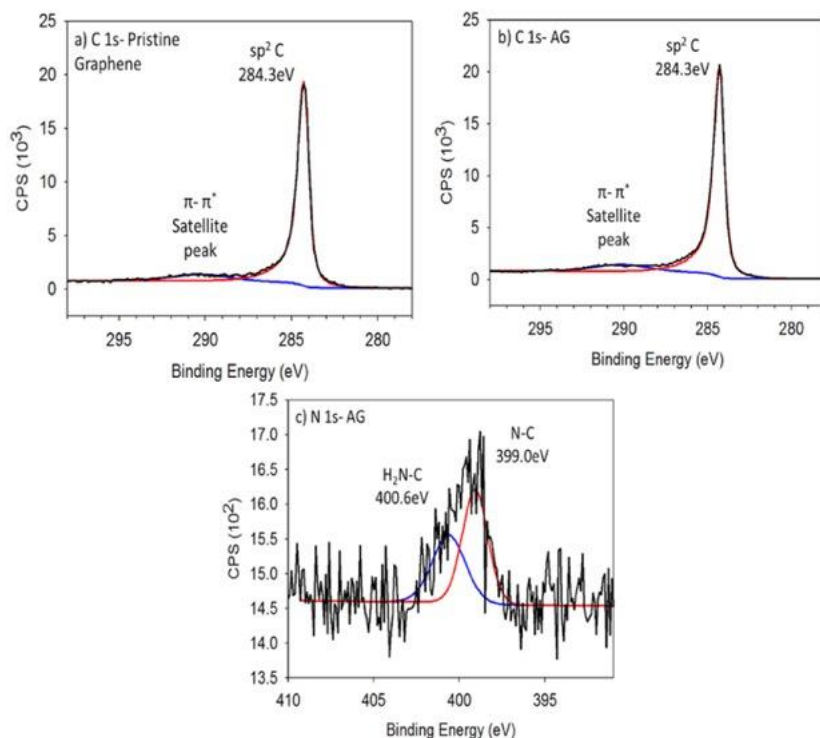


Figure 2.3. XPS spectra of (a) the C1s of MEG and (b) the C1s and (c) N1s of sputtered amine functionalized graphene

Raman analysis performed on both MEG and aminated graphene showed that the introduction of the amine groups increases the disorder of the graphene (Figure 2.4). In all samples a band for disordered, sp³, carbon was observed at ~1350cm⁻¹ and graphitic, sp², carbon at 1550-1600cm⁻¹. The third peak observed at ~2600cm⁻¹ corresponds to the 2D band which is often observed in graphitic material. The position and intensity of this peak can give indication as to the number of

layers present in the material⁶⁷⁻⁶⁹. Each 2D band present in the samples show and asymmetric shape indicating that the graphene is multi-layer. This was determined by calculation of the I_D/I_G ratio of each sample. Pristine graphene had a ratio of 0.30 while aminated graphene had a ratio of 0.95 (Figure 2.4). The increase in I_D/I_G ratio between the MEG and AG samples is due to increasing disorder (i.e. more sp^3 hybridization) present. This increases the number of defects present after functionalization. Perfectly graphitic material has a calculated I_D/I_G ratio of 0 due to the lack of disorder or defects present within the hexagonal lattice or along the edges. A ratio below 1 indicates that the aminated material has still maintained a high degree sp^2 hybridization in the material⁷⁰.

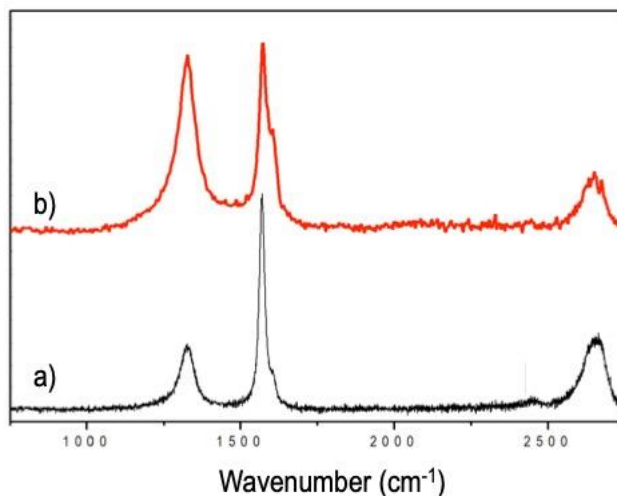


Figure 2.4. Raman spectra of a) MEG and b) AG

Raman analysis of the graphene can allow for the calculation of the crystallite size and domain within the plane of the sample⁷¹. The ratio between D and G was used to determine the L_a , or in plane crystallite size⁷¹. As the amount of disorder (I_D) present in the sample increased there was an observational decrease in the L_a . These values were calculated based on the Raman analysis of each sample. The mechanically exfoliated graphene (MEG) had a calculated L_a of 129.6 nm. After

functionalization the crystallite size decreased, with AG having a calculated L_a of 40.1 nm. As the degree of graphitization present in the AG sample decreases the crystallite size does as well. The decrease in the crystallite size observed in the AG sample is due to the use of a MEG precursor with a smaller size. A smaller crystallite and particle size of the MEG the higher degree of disorder which can be imparted into the material during functionalization⁷².

XRD analysis of mechanically exfoliated graphene and AG is shown in Figure 2.5. The slight shift observed in the pattern of the AG sample is indication that there is slight disruption in the crystalline structure of the pristine material³⁰. Introduction of functional groups on the graphene results in structural changes. Presence of amine groups along the edges disrupt the crystallinity of the graphene, leading to broadening of the peak. XRD analysis gives some indication that the amine groups are present primarily on the edge of the graphene as there is only broadening of the peak and no observable shift.

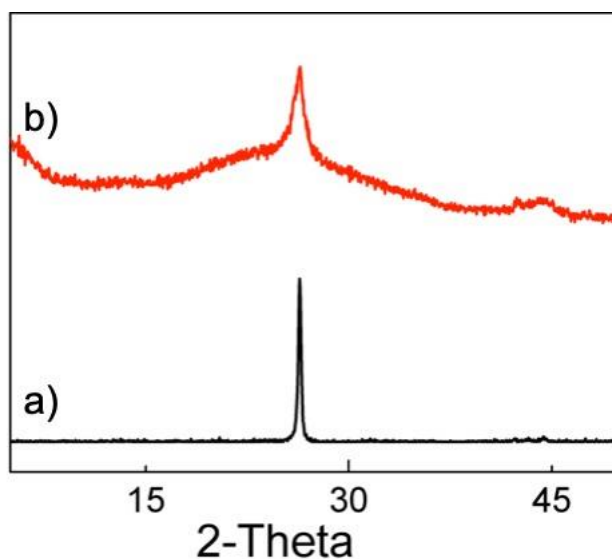


Figure 2.5. XRD pattern of a) MEG and b) AG

Thermal gravimetric analysis was performed under continuous nitrogen flow to analyze the thermal stability of MEG and AG materials (Figure 2.6). MEG displayed little weight loss due to the high degree of thermal stability. TGA analysis of AG shows thermal degradation beginning at approximately 200°C corresponding to the loss of amine groups from the AG (Figure 2.6)⁷³. The continual decomposition observed from 200°-400°C for AG synthesized using pure glycerol as reaction media is an indication that the -NH₂ groups are covalently bonded along the edges versus absorbed on the surface²⁶. Urea shows rapid decomposition at approximately 150°C, no mass loss was observed before or at this temperature for either sample indicating that there was no residual urea present in the AG samples³⁰.

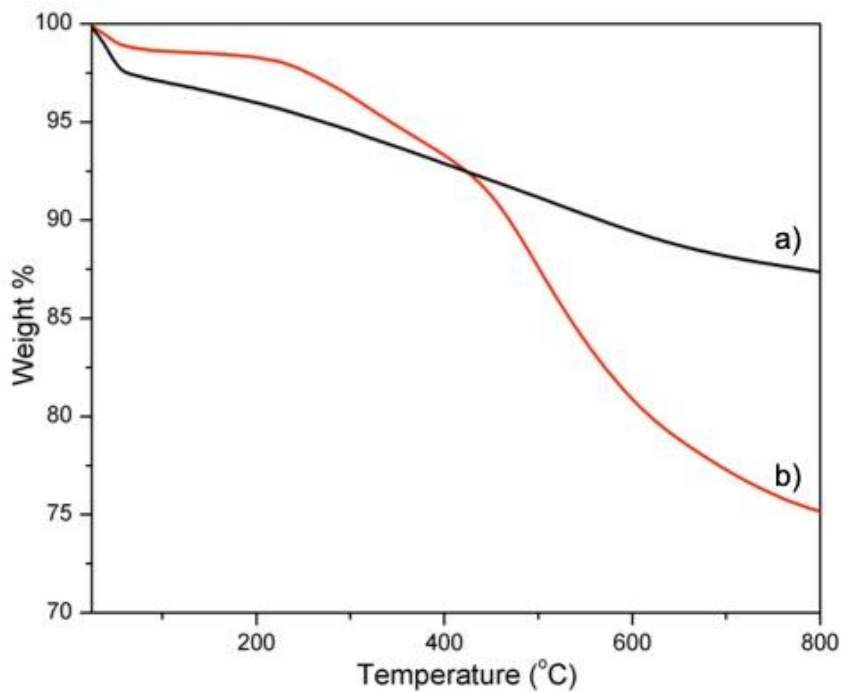


Figure 2.6. TGA analysis of a) MEG b) AG

Dispersion studies were performed on AG samples in order to observe their effects on stability in various organic solvents. Figure 2.7 shows the dispersions in the organic solvents at Day 0 (Figure 2.7) and after Day 60 (Figure 2.7).

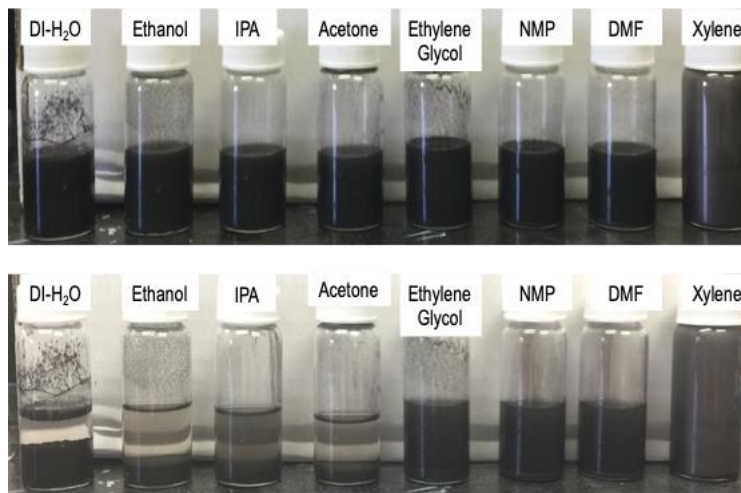


Figure 2.7. AG dispersions at Day 0 (top) and Day 60 (bottom)

It was observed that introduction of $-NH_2$ groups on the surface aided in the dispersion stability in the organic solvents: NMP, DMF, and ethylene glycol (EG). AG in NMP remained dispersed due to interactions between the amine groups on the surface and the conjugated π -orbitals present in the NMP solvent^{28, 58}. Dispersion stability observed with ethylene glycol was due to interactions between the terminal hydroxyl groups in the solvent and the amine groups on the edges of AG. The settlement of AG in water, ethanol, IPA and acetone could be due to the degree of amine groups on the edges of the graphene or weaker hydrogen bonding. Due to the incompatibility between polar amine groups and non-polar solvent systems, AG dispersion in xylenes was not stable. When there are too many polar (*i.e.* amine) groups on the surface of graphene, then it will fall out of dispersion solvents which are more non-polar. Prior studies have performed dispersion

studies on AGO with stability of only up to two weeks whereas this work reports stability of up to two months (60 days)²⁸.

AG in NMP, DMF, and ethylene glycol resulted in the most stable dispersions, but NMP and DMF are considered to be more environmentally hazardous solvents. While ethylene glycol is considered to be the more benign of the three, in order to produce a more environmentally favorable dispersion mixture a low concentration of ethylene glycol is preferred. This was achieved by mixing ethylene glycol with deionized water (DI-H₂O) in varying volume ratios. Two ratios were studied, 1:1 and 1:4 v/v ethylene glycol:DI-H₂O. Dispersion stability was studied for each ratio, maintaining constant AG concentration, in order to establish the minimum amount of ethylene glycol. It was found that at a 1:1 ratio was stable for more than 60 days (Figure 2.8). Stability of the EG:H₂O dispersions were comparable to that achieved with pure EG, NMP, or DMF.

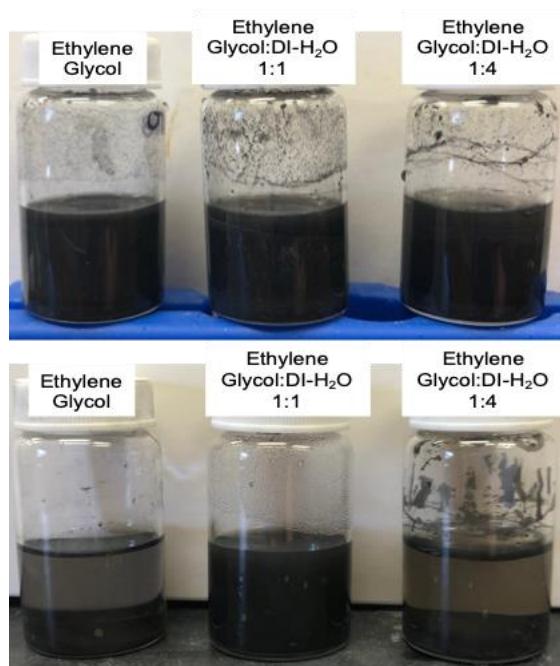


Figure 2.8. AG dispersions in Ethylene Glycol:DI-H₂O at Day 0 (top) and Day 60 (bottom)

2.4 Conclusion

An eco-friendly and low-cost AG synthesis method was developed by directly functionalizing mechanically exfoliated graphene (MEG). This method uses glycerol as a solvent and urea as amination reagent to produce amine functionalized graphene (AG). Through the use of MEG this procedure eliminates the use of hazardous chemicals typically used for synthesis of GO as well as amination of GO. The use of MEG, urea and glycerol at ambient pressure for the amination of MEG makes an eco-friendly and economical one, in line with the practices of green chemistry. FTIR and XPS analysis confirm the presence of $-NH_2$ groups in addition to the presence of C-N bonding. Dispersions in various organic solvents showed that introduction of amine functional groups on graphene helped to enhance dispersion stability in NMP, DMF, and EG. Additionally, we were able to make eco-friendly stable dispersions with mixture of EG and DI- H_2O . These dispersions resulted in prolonged stability (>60 days). Future work aims to apply the synthesized AG for corrosion protection by compositing with 2K urethane or epoxy resins. Reactions between the amine groups on the surface of the AG and isocyanate yield covalent bonds that help to increase the strength of the coatings or composites. We will study the recyclability of the reaction medium.

CHAPTER 3
AMINE AND FLUORIDE FUNCTIONALIZED GRAPHENE
FOR CORROSION RESISTANCE¹

Authors- Melissa A. Wunch^a, Samsuddin F. Mahmood^a, Sangmin Lee^a, and Duck Joo Yang^{ab*}

^a The Department of Chemistry and Biochemistry, BE26

The University of Texas at Dallas

800 West Campbell Road

Richardson, Texas, 75080-3021

^b The Alan G. MacDiarmid Nanotech Institute, BE26

The University of Texas at Dallas

800 West Campbell Road

Richardson, Texas, 75080-3021

¹Manuscript Title: “Amine and Fluoride Functionalized Graphene for Corrosion Resistance”
under review at *Carbon*

Abstract

Recycling of steel coated with sacrificial zinc is an expensive and hazardous process due to acid etching to remove zinc. In order to find a solution to this problem, functionalized graphene materials were studied for corrosion resistance. The multifunctional properties *i.e.* barrier property, high surface area, and hydrophobicity of these materials led to enhanced corrosion resistance when composited with a coating. This study showed a pathway to remove zinc for corrosion resistance of steel substrate. Urethane coating composited with aminated or fluorinated graphene increased corrosion resistance; at 4% concentration the corrosion rate was 0.15 micron per year (mpy) and 0.03 mpy, respectively.

3.1 Introduction

Different methods have been used for corrosion protection of steel substrates.^{63, 74-75} Zinc coated on the surface of a steel substrate is the most widely used method for corrosion protection.⁷⁶⁻⁷⁸ The zinc layer acts as a sacrificial barrier and is consumed over time upon interaction with the environment (*i.e.* oxygen, water, and ions).⁷⁸⁻⁸⁰ Once the sacrificial zinc is exhausted, all layers must be removed before the re-application of coating. This requires the substrate to be completely re-coated, leading to an increase in cost.^{42, 64, 79-81} Additionally, the use of sacrificial zinc makes it difficult to recycle the steel substrate. Expensive and hazardous acid etching using concentrated sulfuric acid (H₂SO₄) is used to remove the zinc layer from used car bodies in order to recycle them.⁶⁴ Replacing zinc with an alternative material, *e.g.* graphene, can be a potential solution for this problem because of its barrier and hydrophobic property.^{50, 53, 82-83} Elimination of sacrificial zinc layer will enable the steel substrate to be easily recycled since a graphene contained polymer

coating can be readily removed by decomposition at molten steel temperature (1370-1510°C). This leads to a more economical and environmentally benign means of recycling steel.

Graphene is single layer carbon based material with properties such as: hydrophobicity, high surface area (2630 m²/g), high conductivity, chemically inertness and enhanced barrier property.^{47, 19, 21, 49, 54, 84} These multifunctional properties allow this material to be of interest in various fields such as electronics, nanotechnology, or corrosion protection.^{46-47, 49, 54, 57, 84} However, pristine graphene material has disadvantages of no covalent bond formation with polymer matrices.^{49, 84} This disadvantage can be overcome through surface functionalization of graphene to alter its properties. For example, amine functionalized graphene can react with epoxy group or isocyanate group from polymer resins. Introduction of fluoride functionalized graphene enhances hydrophobicity of polymer coating.^{28, 50, 53, 58-59, 85} Addition of graphene into urethane or epoxy based coatings can provide a torturous pathway for oxygen (O₂), water (H₂O) molecule or ions to pass through before reaching the steel surface.^{50, 56, 86-87} This is due to the availability of multi-level 2D graphene in coating layer. Thickness of single layered graphene is about 3 Å while that of coating layer is about 30 μm. This study is about the effect on corrosion resistance by introduction of amine or fluoride functionalized graphenes to a polymer coating.

Graphene oxide functionalized with amine groups (-NH₂) on the surface is known as aminated graphene oxide (AGO).^{34, 73} This type of functionalization has been performed using various different methods, with varying amine sources.^{30, 32-34, 36} The graphitic starting material is pretreated using the Modified Hummer's method to synthesize graphene oxide (GO) prior to amination.^{19, 34, 61, 88-89} This material can then go through different synthetic pathways in order to attain the final amine functionalized material.^{22, 32, 34, 61, 90} Tetsuka *et al.* synthesized AGO material

using urea as the amine source.⁹¹ This AGO was produced through treatment of a GO dispersion in aqueous urea using a high-pressure autoclave.⁹¹ Application AGO has been studied in a wide range of fields. One field this material has been studied is for corrosion protection. The amine groups can react with epoxy groups present in resins. AGO has gained interest as a potential material for corrosion protection.³⁴ Ramezanzadeh *et al.* studied the effect that AGO functionalized with *para*-phenylenediamine (PPDA) had on barrier and corrosion protection upon addition to an epoxy based coating.³⁴ While many have reported the use of AGO with epoxy based coating, few have looked to its effect when composited with urethane. In this study the use of AG is studied in a 2K urethane coating system and its effect on corrosion resistance.

Additionally, fluorinated graphene materials have been of recent interest due to their ability to widen the band gap of graphitic material and to increase its stability.^{18, 38-39, 59, 85, 92} Similar to aminated graphene, fluorination of graphene has been synthesized, commonly with chemically exfoliated graphene containing oxygen functional groups, using different methods.^{18, 29, 38-39, 47, 59,}⁹³ Graphitic materials can be fluorinated by direct gas fluorination, using XeF₂ or F₂ gas as the fluorination source.^{18, 20, 29, 38, 94} Mazanek *et al.* uses a 20% F₂/N₂ gas mixture to perform fluorination on GO.³⁸ Their research showed that through adjusting different experimental parameters (*i.e.* temperature and time), it was possible to adjust the fluorine content in the final product.³⁸ Research into FG as an additive in coatings for corrosion protection has been studied primarily in epoxy based coating systems. Yang *et al.* deposits synthesized fluorinated graphene oxide (FGO) on the surface of an epoxy coating to aid in corrosion protection.⁴⁰ Due to the polar nature of the fluoride groups on the surface, they are able to enhance surface properties and corrosion protection. While FGO was able to provide enhanced corrosion protection, the lifetime

of the composite coating can be limited due to the surface coating with FGO. There are few works which study the effect fluorinated graphene materials on surface and corrosion protection when included within the coating matrix. The work outlined below shows how FG, when dispersed within the 2K urethane coating, effects on the surface properties and corrosion resistance.

This study reports the use of AG and FG as a barrier for corrosion resistance composited with a two-component (2K) urethane coating. Both AG and FG were dispersed within the coating to form composite coatings. These coatings were directly applied on a steel substrate to monitor their effects on the corrosion resistance capability. Surface properties (*i.e.* hydrophobicity) and corrosion resistance of composite coatings made with AG and FG were quantitatively measured. Results outlined below describe how both AG and FG can lead to promising alternative materials for corrosion resistance. These results show a direction towards the potential elimination of zinc layer from galvanized steel substrates.

3.2 Materials and Methods

Materials

Graphene nanoplatelets (99% Carbon) were purchased from xG-Sciences company. Stainless steel substrates (SAE304 Grade, 70mm x 150mm) and 2K urethane organic binder solutions, acrylic polyol (AP) and urethane curing agent (UCA), were provided by Kangnam Jevisco Co., LTD in Korea. Fluorine (5% F₂/N₂) gas was purchased from NOVA Gas. Ethylene glycol (99%, ACS Grade), Urea (99%, ACS grade), and Hydrochloric Acid (HCl, concentrated, Technical grade) were purchased from Fisher Scientific. Potassium Bromide (KBr, FTIR grade) was purchased from Sigma Aldrich. All chemicals and materials were used as received without purification.

Synthesis of Amine Functionalized Graphene (AG)

Amination of graphene nanoplatelets was performed using a facile reflux method at 1 atmospheric pressure. Urea served as the amine source for amine functionalization. 1g of urea was added to a 250mL round bottom flask, followed by the addition of 1g of graphene. After addition of urea and graphene, 100mL of ethylene glycol (EG) was added and the solution was stirred at room temperature for 30 minutes. After stirring, the solution was heated to 190°C, under reflux, and ran for 5h. The reaction was allowed to cool to room temperature on its own before filtration and purification.

Synthesis of Fluorinated Graphene (FG)

Graphene nanoplatelets were fluorinated through direct gas fluorination. Graphene was placed in a reactor, which was purged with N₂ gas to react a pressure of 15PSI. It was kept at 15PSI for approximately 15 minutes for equilibration. The chamber was then charged with a 5% F₂/N₂ gas for 24h. It was then purged with N₂ gas in order to remove excess F₂ and HF species present. The sample was then removed from the reactor.

2K Urethane Coating Preparation

Functionalized graphenes were included directly to a two-component (2K) urethane coating by method of probe sonication (Hielscher). Amine and fluoride functionalized graphene were dispersed in acrylic polyol (AP) followed by the addition of an isocyanate-based curing agent (UCA). AP and UCA were mixed in a 4:1 (v/v) ratio. The coating was then applied directly onto a steel substrate for surface and corrosion analysis. Graphene nanoplatelets (G), AG, and FG were included at concentrations of 1, 2, and 4% by weight of solids in the resins.

3.3 Characterization

Physical and Chemical Characterization

Characterization of functionalized graphene materials were performed using qualitative and quantitative methods to confirm the functionalization of graphene. Fourier infrared spectroscopy (FT-IR) was performed using KBr with a range of 400-4000 cm^{-1} on a Perkin-Elmer Spectrometer. Functionalized graphene was also analyzed using elemental analysis by sending to Galbraith Labs. Raman spectroscopy was performed on all graphene samples using a Jobin Yvon LabRam HR Micro-Raman Spectrometer with 633 nm laser. Thermogravimetric analysis (TGA) was performed on all samples using a Q600 simultaneous TGA/DSC instrument ramped up to 800°C at a rate of 10°C per minute under nitrogen (N_2).

Contact Angle Characterization

Contact angle measurements were collected with a Dataphysics-OCA goniometer. Contact angle measurements were taken in triplicate in order to establish an average measurement and standard deviation.

Corrosion Resistance Measurements

Corrosion analysis was performed following ASTM G1 standards, through immersing each sample in a 3.5% NaCl bath for 60 days. These samples were then rinsed with concentrated HCl and DI- H_2O in order to remove any excess rust from the surface.

Impedance (EIS) Measurements

Corrosion protection study was performed through electrochemical analysis using electrochemical impedance spectroscopy (EIS). Measurements were carried out on a PARSTAT 2273 impedance analyzer. The EIS measurements were taken under OCV at a frequency range of 1MHz to 10mHz

with an alternating current of 10mV. These analyses were performed using a three-electrode set-up with the steel coated sample serving as the working electrode, Pt-mesh as the counter, and a saturated Ag/AgCl reference electrode. Each of these measurements were performed in triplicate so as to ensure reproducibility of results.

3.4. Results and discussion

Characterization of Amine and Fluoride Functionalized Graphene

Characterization of aminated and fluorinated graphene samples were done using FT-IR, Raman, and TGA to confirm presence of amine and fluoride functional groups. FT-IR analysis of AG confirmed functionalization by N-H stretching vibrations present at 3500-3650 cm^{-1} and 1550 cm^{-1} and the stretching vibrations of aromatic C-N at 1084 cm^{-1} (Figure 3.1a). Presence of the C-F vibrational band at 1071 cm^{-1} indicates that fluoride groups are present (Figure 3.1b).

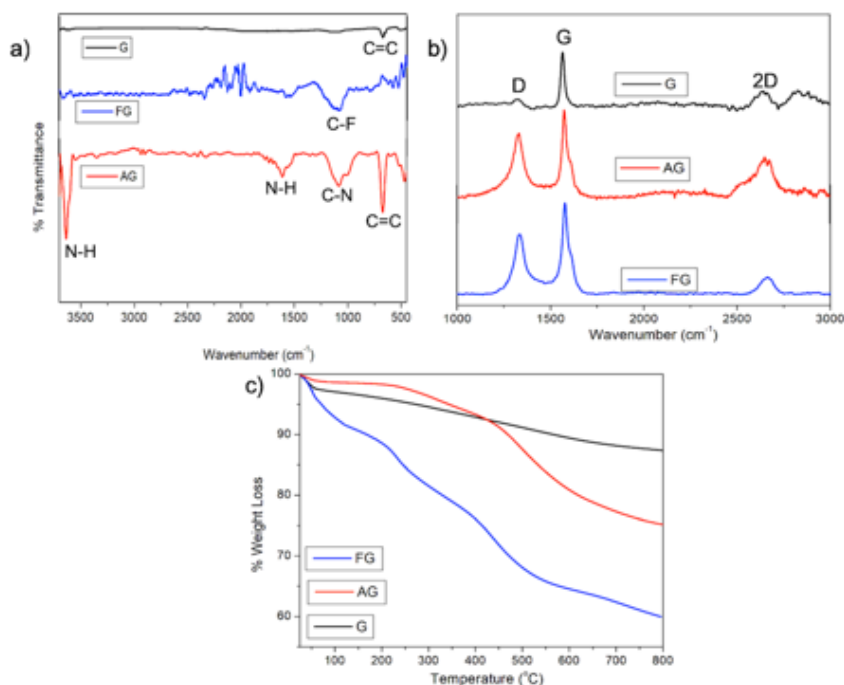


Figure 3.1. Characterization of functionalized graphenes. (a) FTIR, (b) Raman spectra showing characteristic D and G bands, and (c) TGA of G, AG, and FG graphenes

Disorder of the graphitic backbone caused by functionalization was analyzed using Raman spectroscopy of G, AG, and FG. In order to determine how disordered the graphene is the ratio of the D and G bands are taken as I_D/I_G . The higher the G content present in the material the higher the graphitic, or sp^2 , content. Calculated I_D/I_G ratio for G is 0.2 (Figure 3.1c). This value increases after functionalization indicating a disruption in the graphitic backbone. The ratio for AG was calculated to be 0.4 and for FG the ratio was calculated to be 0.3 (Figure 3.1c). Increase in the I_D/I_G ratio observed in AG and FG confirms that graphene was functionalized. Thermal gravimetric (TGA) also shows success of functionalization (Figure 3.1d). These functionalized materials were added to a two-component (2K) urethane-based coating system to test for corrosion protection.

Coating Surface and Corrosion Analysis

The 2K urethane coatings were applied onto steel substrates, after which contact angle measurements for each sample were taken. Figure 3.2 shows contact angle measurements as a function of increasing graphene concentration. It was observed that addition of graphene to the coating helps to enhance the hydrophobicity of the coating. As the concentration of graphene increases, the more hydrophobic the surface becomes. In the case of FG, the presence of highly polar fluoride groups on the surface increases the hydrophobicity versus G.

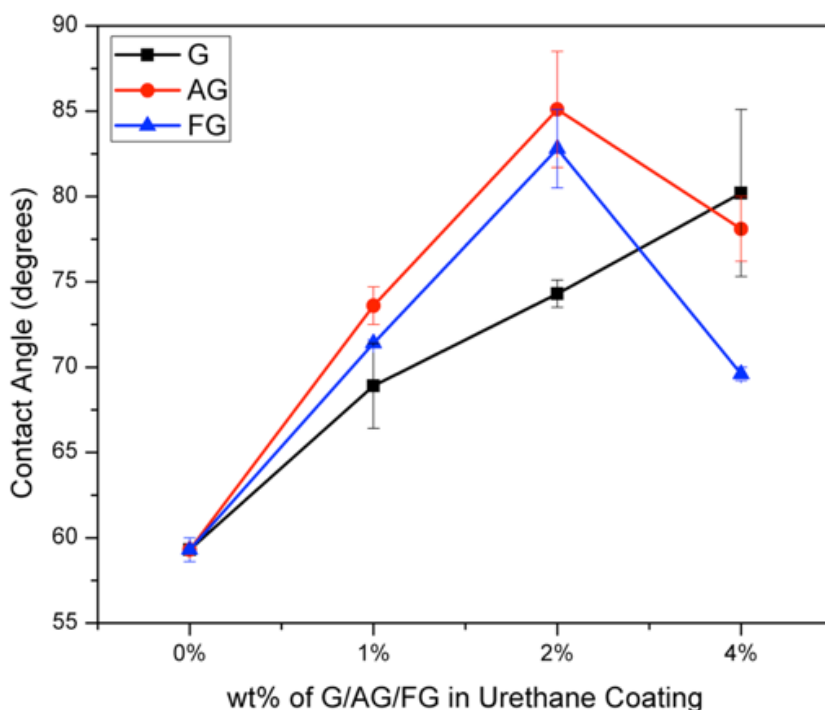


Figure 3.2. Contact Angle Measurements of G, AG, and FG in 2K Urethane Coating as a function of increasing graphene content.

The contact angle at 1% by weight concentration is increased by 7% and 4% when AG or FG is added respectively. Increasing the concentration to 2% AG or FG showed an increase of 15% and 12% respectively. Further increase in concentration to 4% of AG there was a decrease in contact angle. The decrease observed for AG is due to the increase of polar groups on the surface. This is because the additional amine group on the graphene reacted with isocyanate groups in the coating, which produced a more polar surface. At 4% FG there was a further increase in contact angle to 91°. Based on this study a concentration of 4% for both AG and FG is the optimal concentration to achieve high hydrophobicity.

Corrosion and Impedance Characterization Corrosion analysis was performed following the ASTM G1 standard. Each coated steel substrate was immersed in a 3.5% NaCl solution for 2

months. They were then rinsed with concentrated HCl and DI-H₂O in order to remove excess rust.

Figure 3.3 shows coated substrates after 2-month immersion in 3.5% NaCl solution.

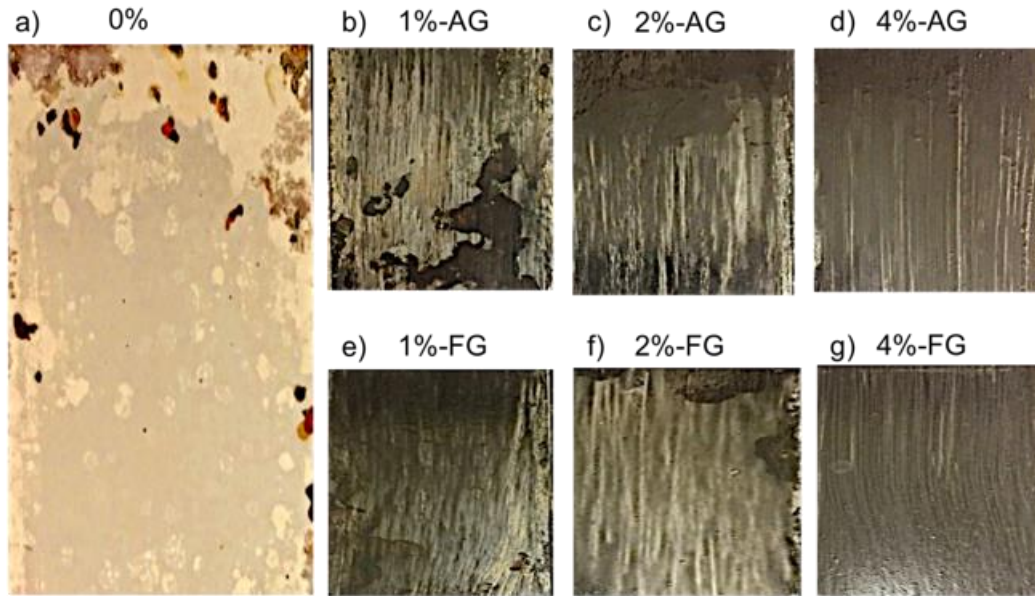


Figure 3.3. Corrosion results of (a) 0%, (b-d) 1, 2, and 4wt% AG, and (e-g) 1, 2, and 4wt% FG. Observations indicate that no use of graphene lost all coating from surface, and as concentration of the functionalized graphene increased, the corrosion decreased.

In general, as the concentration of graphene increases, the corrosion rate decreases (Figure 3.4).

Figure 3.4 shows that addition of functionalized graphene to the urethane coating provides enhanced corrosion protection. Among G, AG, and FG, both functionalized graphenes are better in corrosion protection compared to G. Figure 3.4 shows that addition of functionalized graphene to the urethane coating provides enhanced corrosion protection. Among G, AG, and FG, both functionalized graphenes are better in corrosion protection compared to G.

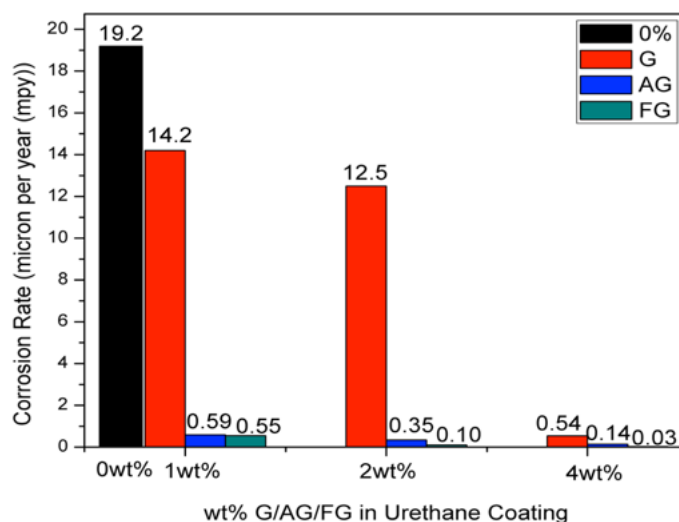


Figure 3.4. Corrosion rate comparison: 0% vs. G vs. AG vs. FG. These results indicate that functionalized graphene enhances corrosion protection.

G , at 1wt%, showed a decrease of 26% in corrosion rate, with respect to 0%, no use of graphene. Increasing the concentration to 4% further decreased the corrosion rate by 97% with respect to 0%. When aminated graphene was compared to G for corrosion resistance, the corrosion rate with AG use decreases by 96% and 74% at concentrations of 1% and 4% respectively. At a concentration of 1%, fluorinated graphene decreased the corrosion rate by 96% compared to G. Increasing the concentration of FG from 1% to 4% decreases the corrosion rate by 94% compared to pristine graphene. The rates between AG and FG samples were then compared. The corrosion rate decreased by 7% upon addition of AG versus FG at a concentration of 1wt%. Increasing the concentration to 2wt% AG versus FG decreased the rate by 71%. At a concentration of 4wt% addition of AG decreased the corrosion rate by 78% when compared to FG. Corrosion study results show that both AG and FG are better than 0% and G for corrosion resistance. Between AG and FG, FG is better for corrosion resistance.

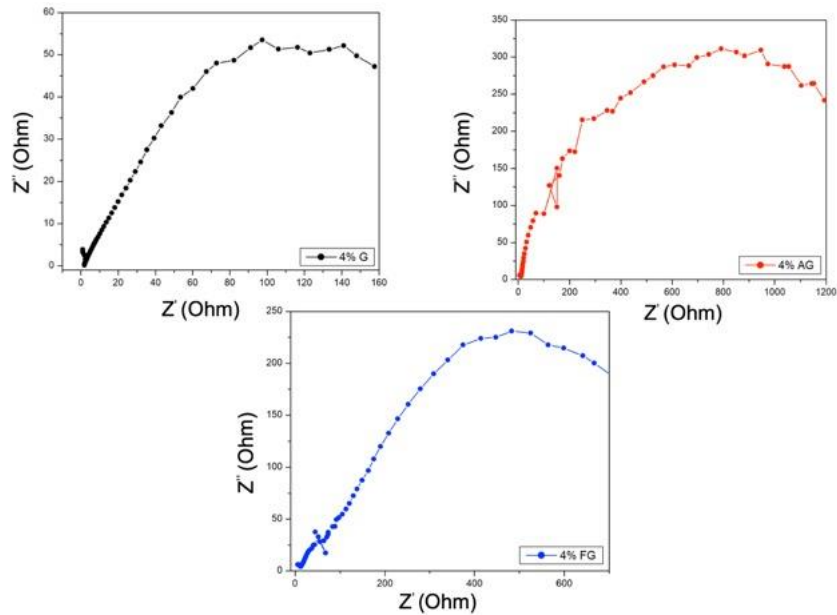


Figure 3.5. Impedance Data from EIS analysis of 4% G, 4% AG, and 4% FG coated substrates. Each sample had exposure in a 3.5% NaCl solution for 60 days.

The Nyquist plots for 4% G, AG, and FG samples after immersion in 3.5% NaCl for 60 days are displayed in Figure 3.5. Impedance analysis of these coatings allows for the understanding of the mechanism in which the graphenes are providing corrosion protection. Analyzing each frequency range can indicate the reaction occurring at the interface of the metal/coating and how it is affecting the coating's properties. It was observed that the Z' frequency for the 4wt% AG sample is higher than 4wt% G or FG. While frequency of FG is lower than AG, it is still higher than G. This is indication that the coating has retained high barrier and strong interfacial bonding, decreasing the amount of electrolyte penetrating the coating. Adhesion properties of the coating are an important aspect to maintain the barrier performance, therefore based on impedance data AG provides a higher degree of corrosion resistance versus G and FG.

3.5. Conclusion

Two different functionalized graphene materials were studied for their effect on corrosion resistance when included in a urethane coating. Based on this study, optimum use of both AG and FG at 4% concentration in urethane coating is important to achieve the best corrosion performance. Considering barrier and hydrophobic property of functionalized graphenes as well as compatibility between the functionalized graphenes and coating solution is important to achieve optimal corrosion protection. At 4wt% concentration aminated graphene showed a corrosion rate of 0.14 mpy, while fluorinated graphene had a rate of 0.03 mpy. While both displayed enhanced corrosion protection, based on cost of functionalization and impedance performance (adhesion) of functionalized graphene composite coating, aminated graphene (AG) use is preferred. The use of these functionalize graphenes in urethane coatings outlines a step towards the potential removal of zinc from steel. This will allow used steel products (i.e. automotive bodies) to be readily recyclable. Our future work in this area aims to use mixtures of AG and FG, as well as a functionalized graphene containing both amine and fluoride groups for corrosion resistance.

II. SYNTHESIS OF VANADIUM NITRIDE-CARBON NANOFIBER MATS AND THEIR APPLICATION FOR ASYMMETRIC SUPERCAPACITOR ELECTRODES

CHAPTER 4
INTRODUCTION: TRANSITION METAL OXIDES AND NITRIDES
FOR ENERGY STORAGE

Due to the increase in energy consumption in the last decade and growing demand of electrical vehicles, there has been an increase in research to develop materials with enhanced energy storage capabilities. Additionally, there has been much research towards the development of alternative energy sources to reduce greenhouse gas emissions. These sources include wind or solar energy, geothermal, hydrogen, and hydroelectric⁹⁵. Currently, there is significant difference between energy output and energy demand⁹⁵⁻⁹⁶. In order to overcome this discrepancy, it is necessary to develop materials which can have a fast rate of charge with slow rate of discharge. This can be achieved by the development of more efficient energy storage materials and/or devices⁹⁷. Current devices, such as Li-ion batteries and electrolytic capacitors (capacitors), have the potential to provide the necessary energy and power to meet demands⁹⁷. Figure 4.1 outlines a Ragone plot which shows the relationship between the power and energy density of current energy storage devices.

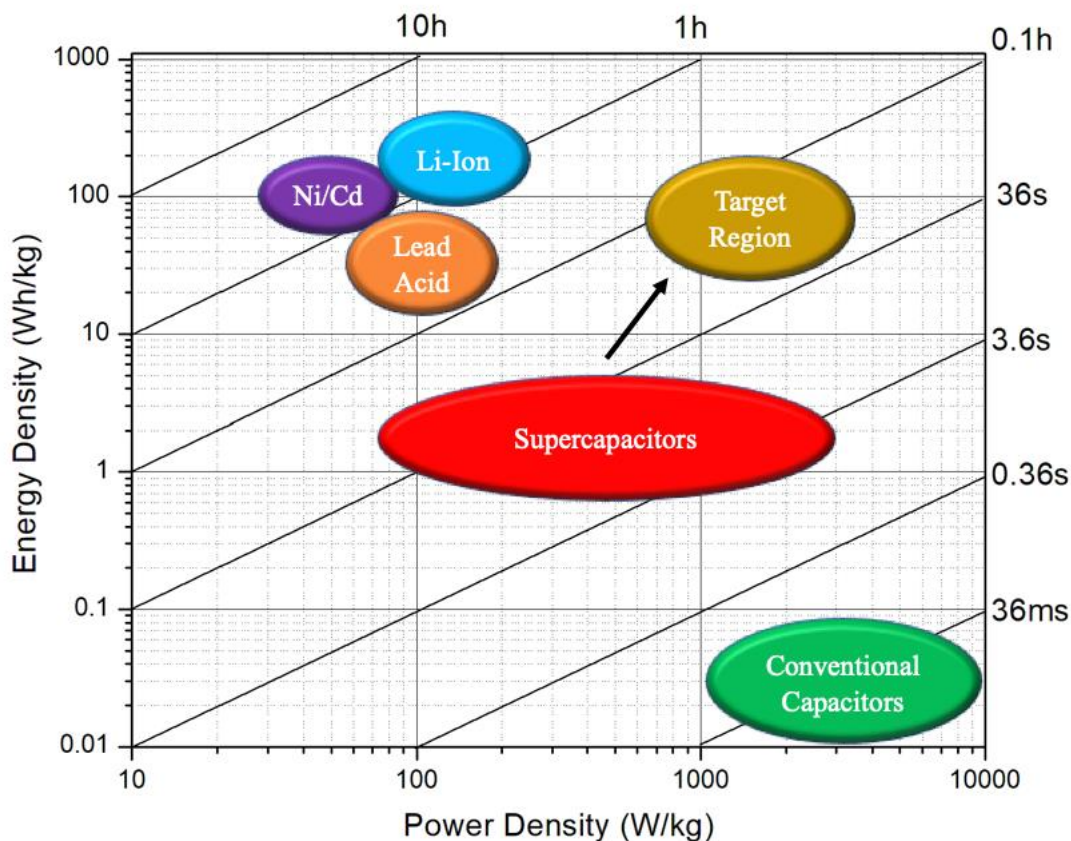


Figure 4.1. Ragone Plot

While Li-ion batteries can provide high energy densities, they suffer from low power densities. Conversely, capacitors provide high power but suffer from low energy densities. This has led to the development of supercapacitors. These have garnered increased interest due to their ability to bridge the gap between Li-ion batteries and conventional capacitors.^{95,97} Supercapacitors can be broken down into three primary categories depending on the charge storage mechanism. Figure 4.2 displays the different categories of supercapacitors and how they store charge.

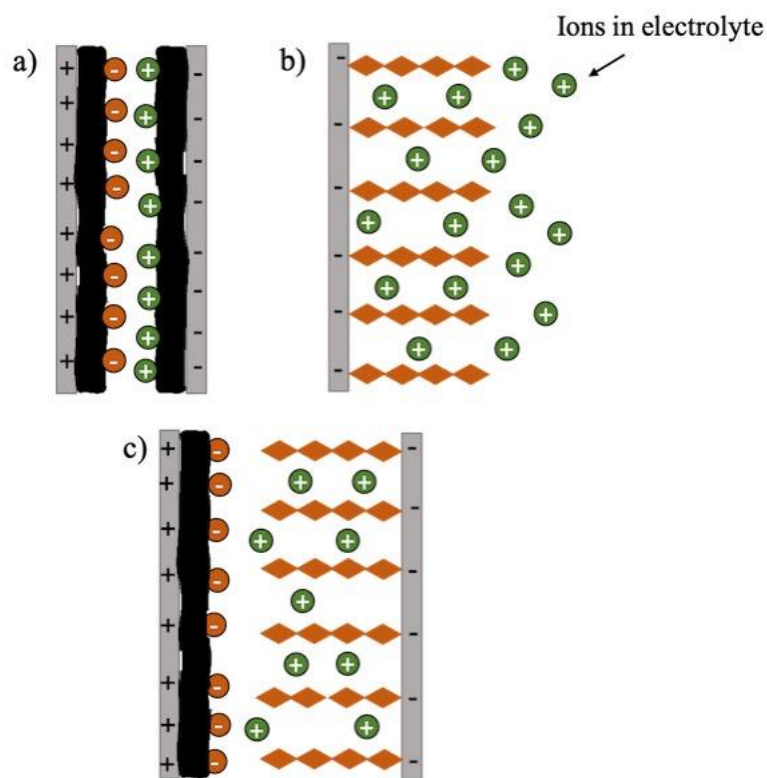


Figure 4.2. Pictorial representation of the charge storage mechanism for each category of supercapacitor. (a) EDLC, (b) intercalative pseudocapacitor, and (c) hybrid

Electrochemical double layer capacitors (EDLC) consist of high surface area and conductive carbon materials⁹⁶. These devices store charge through electrostatic mechanisms on the surface of the electrodes (Figure 4.2a)⁹⁶. The second category includes pseudocapacitors, which consist of redox active metal oxides or metal nitrides with conductive materials. Oxides and nitrides are combinations of a transition metal (V, Mn, Ru, etc.) with oxygen or nitrogen. Common transition metal oxides (TMOs) studied for pseudocapacitors are vanadium oxide (V_2O_5), ruthenium oxide (RuO_2), manganese oxide (MnO_2), etc^{95, 98}. Transition metal nitrides (TMNs) studied for energy storage include vanadium nitride (VN), titanium nitride (TiN), molybdenum nitride (MoN), or tungsten nitride (WN)⁹⁹⁻¹⁰⁰. These devices store charge through surface redox reactions or

intercalative processes (Figure 4.2b)⁹⁵. Some pseudocapactive materials, such as metal oxides, suffer from low conductivity which can be overcome by making composites with EDLC materials. This is the third area of supercapacitors known as hybrid capacitors. Hybrids can be broken down into two categories: asymmetric or composite. Asymmetric hybrid devices combine EDLC materials as the cathode and pseudocapactive materials as the anode (Figure 4.2c).

Composite hybrid electrodes are a combination of EDLC and pseudocapactive at the anode with EDLC material at the cathode⁹⁵. The conductive carbon can help to overcome the low conductivity observed in some metal oxides (i.e. vanadium oxide) or overcome the low stability observed in some metal nitrides (i.e. TiN or VN).

Capacitance is directly related to the amount of stored charged, as shown in equation 4.1. It is related in terms of charge (Q) per unit voltage (V). The more charge (Q) the material is capable of storing the higher the capacitance. It can also be increased by increasing the surface area of the electrode material. Equation 4.2 outlines how surface area (A) and capacitance (C) are directly related to one another. Dielectric constants for electrolyte and vacuum are denoted as ϵ_0 and ϵ_r , respectively.

$$\text{Eqn. 4.1. } C=Q/V$$

$$\text{Eqn. 4.2. } C= \epsilon_0 \epsilon_r \frac{A}{d}$$

Capacitance is also directly related to the energy density of the material as outlined in equation 4.3. By increasing “C” of the material it is possible to increase the energy of the device.

However, another variable in the equation is voltage (V). Through using electrolytes which can increase the operating voltage window the energy can increase quadratically.

$$\text{Eqn 4.3. } E= \frac{1}{2} CV^2$$

Compositing TMOs or TMNs with high surface area and conductive carbons can help to overcome obstacles which hinder performance (e.g. conductivity)^{95, 98-99}. Amongst the TMOs studied, RuO₂ offers high capacitance (~1500 F/g) and conductivity (2.8x10⁶ S/m); however, its high cost has limited its use in commercial devices¹⁰¹. This has led to research into alternative metal oxides, such as V₂O₅, for energy storage. Vanadium oxide is low cost and can exist in multiple oxidation states, however it suffers from low conductivity (1.0x10⁻⁴ S/m)⁹⁸ and capacitance. In order to overcome this, V₂O₅ is often composited with a conductive carbon (e.g. graphene, activated carbon, carbon nanofibers, etc.) which helps to enhance the conductivity and capacitance^{95, 98}. While TMNs offer higher conductivity, several suffer from stability issues when used in the bulk⁹⁹. VN based electrodes have been studied as an anode material for pseudocapacitors. VN provides high conductivity (1.23x10⁶ S/m) and theoretical capacitance (~1350 Fg⁻¹), which are both significantly higher than what has been reported for V₂O₅⁹⁹⁻¹⁰⁰. Composite electrodes with VN have also been studied, however research has been aimed towards encapsulating the VN within the carbon versus deposition on the surface^{99, 102-103}. This is due to the low stability of VN when in the presence of electrolytes, which leads to the formation of VNOH¹⁰³⁻¹⁰⁴.

Metal Oxide/Metal Nitride-Carbon Composite Electrodes

As stated previously vanadium oxide, while cheaper than RuO₂, suffers from low conductivity and capacitance⁹⁸. In order to overcome this obstacle several studies have been aimed at making V₂O₅-Carbon composites. Carbon materials used in these composites include graphene, carbon black, carbon nanofibers (CNF), or templated carbons¹⁰⁵⁻¹⁰⁷. An alternative to composite electrodes to have increased capacitance, researchers have studied vanadium nitride (VN) since it

will enhance both conductivity and capacitance, as a means to overcome the limitations presented by V_2O_5 .

Vanadium oxide is transformed to the more conductive nitride, VN, through a process called nitridation¹⁰⁸⁻¹¹⁰. This treats the oxide with ammonia (NH_3) gas at an elevated temperature for a certain time period to produce the nitride^{108, 110}. VN offers the cost benefits of using vanadium oxide, while providing conductivity and electrochemical properties comparable to those of RuO_2 ¹⁰⁰. During the nitridation process V_2O_5 transitions to V_2O_3 which is the final oxide phase that undergoes nitridation. The balanced chemical reaction between V_2O_3 and NH_3 is displayed in Scheme 4.1.



Scheme 4.1. Reaction between $V_2O_{3(s)}$ and $NH_{3(g)}$

While VN has high conductivity and theoretical capacitance, the bulk material suffers from long term stability in energy storage devices¹⁰⁰. This means that upon cycling the material for multiple cycles (>500) at a constant current (>1A/g), it degrades rapidly and results in low retention (~50%). In order to overcome this obstacle, many have researched to develop composite materials in which the VN is encapsulated within the carbon, hence avoiding direct interaction with the electrolyte^{108, 111}. An *et al.* reported the encapsulation of VN in carbon nanofibers to produce supercapacitor electrodes with high stability¹⁰³. Through tailoring the concentration of VN with the type of carbon it is possible to develop a hybrid device with high conductivity, long cycle stability, and high energy and power density.

Electrolytes: Aqueous, Organic, and Ionic Liquid

There are different types of electrolytes used in energy storage devices: aqueous, organic, and ionic liquid. The most commonly reported is the use of an aqueous electrolyte. These electrolytes include KOH, KCl, Na₂SO₄, Li₂SO₄, etc. While they offer the benefit of low cost, they have a limited voltage window ~1V. However, recent work has been aimed at developing aqueous based electrolytes which can operate at wider potential windows (1.5-2.5V)¹¹²⁻¹¹³. Some electrolytes which have been studied are sodium sulfate (Na₂SO₄) and water-in-salt (WIS)^{112, 114-116}. Organic electrolytes offer the potential to provide a wider potential window while operating devices¹¹⁷. They are often composed of an organic salt (TEA-BF₄) dissolved in acetonitrile (ACN) or propylene carbonate (PC)¹¹⁸⁻¹¹⁹. These electrolytes offer an average operating voltage window of ~2.5V, approximately 2.5x increase versus aqueous electrolytes. The main drawback to the use of organic electrolytes in devices is the toxicity related to the solvent, and their flammability¹¹⁹. Ionic liquid electrolytes are the third type of electrolyte used in supercapacitors^{52, 120-121}. These electrolytes offer an operating voltage window of >3.5V¹²¹. As stated earlier, by increasing the operating voltage (V) window the energy density will increase quadratically ($E=1/2CV^2$). Enhancing the V in the equation from V=1.0V to V=3.5V can lead to a 12.25-fold increase in energy density. There are different types of ionic liquids available to use, including EMIM-TFSI, Pyr₁₃TFSI, or Pyr₁₄TFSI, which provide a non-flammable alternative to organic electrolytes¹²¹. Figure 4.3 displays the structures of the different ionic liquids, which can be matched to the material being used in the device¹²².

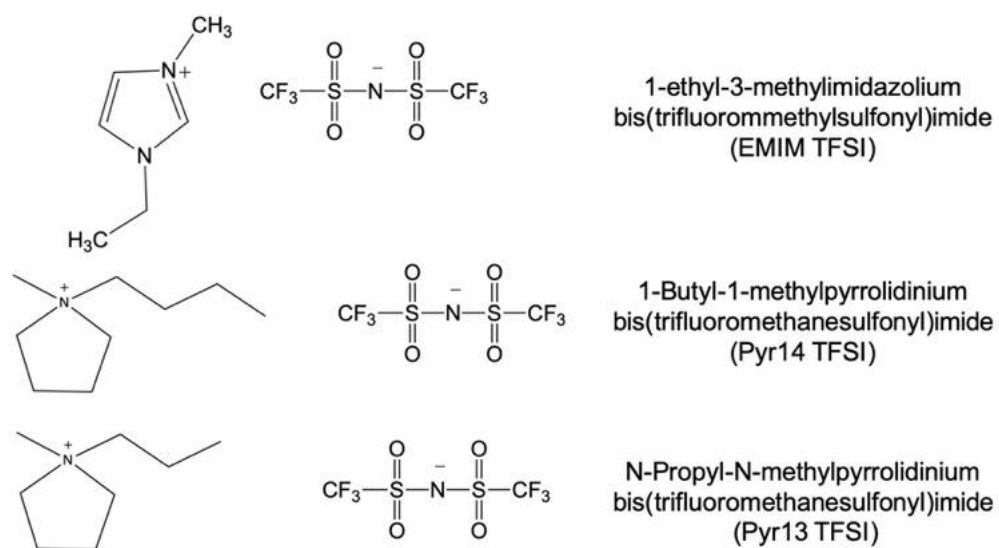


Figure 4.3. Structures of ionic liquid electrolytes commonly studied in supercapacitors

While each of the electrolytes described above provides a wider operating window, it may be necessary to adjust it depending on the material being studied (e.g. metal oxides, metal nitrides, etc.)^{120, 122}. If the operating voltage window exceeds what the material can handle, it can degrade during testing. Correct selection of ionic liquid electrolyte for VN based pseudocapacitors, it may be possible to overcome the surface oxidation of VN.

CHAPTER 5

VANADIUM NITRIDE-CARBON FIBER (VN-CF) COMPOSITE ELECTRODES FOR ASYMMETRIC SUPERCAPACITOR ELECTRODES

5.1 Introduction

Development of efficient energy storage devices has been of interest in the last decade due to the depletion of fossil fuels and increased interest in renewable energy⁹⁵. Among these devices, supercapacitors have attracted attention recently due to their ability to help bridge the gap between conventional Li-ion batteries and electrolytic capacitors. Supercapacitors provide high energy and high power, in addition to their safe operation at a wide range of temperatures and voltages⁹⁵. Capacitance is the amount of charge (Q) stored per unit voltage (V), or $C=Q/V$. This can also be related to energy density, where $E=1/2CV^2$. There are three main categories of supercapacitors: electric double layer capacitor (EDLC), pseudocapacitor, and composite. EDLC supercapacitors have porous carbon materials as their electrodes¹²³⁻¹²⁴. These are the most commercially available supercapacitors; however, their energy storage and capacitive capabilities are limited due to limited access to the surface¹²⁴. Pseudocapacitive materials, however, can achieve high energy and power densities due to the intercalative and surface redox processes occurring in the material. However, the relatively low conductivity of some of the anode materials has limited the commercial viability for these materials. Electrodes in pseudocapacitors consist of redox active materials, such as metal oxides, metal nitrides, or conductive polymers. Due to the limitations presented by some of these materials (e.g. cost or low conductivity) studies have looked to composite them with porous and conductive EDLC materials⁹⁵. Transition metal oxides or nitrides (e.g. V_2O_5 , RuO_2 , MnO_2 , TiN , VN , etc.) have

been studied as electrode material due to their redox capabilities^{99-100, 125-126}. Amongst these RuO₂ has the capability to produce high capacitance, due to its high conductivity, however its high cost and toxicity has limited its use commercially. This has led to research into cheaper, alternative materials, like vanadium oxide (V₂O₅) or nitride (VN)⁹⁸⁻⁹⁹. Transition metal nitrides, such as VN, TiN, MoN, or WN, offer high conductivity which makes them a promising electrode material⁹⁹⁻¹⁰⁰. Conductivities for these materials can range from 4.0x10⁵-5.5x10⁶ S/m⁹⁹⁻¹⁰⁰.

Vanadium oxide has garnered significant interest because of its low cost, ease of synthesis, and ability to exist in multiple oxidation states (V²⁺, V³⁺, V⁴⁺, or V⁵⁺)⁹⁸. However, it suffers from low conductivity and cycle stability⁹⁸. Research has been done in order to help overcome these obstacles through developing composite electrodes with EDLC materials and V₂O₅. Kim *et al.* synthesized composite electrodes using V₂O₅ nanofibers and carbon nanofibers (CNFs)¹⁰⁷. Their results showed a capacitance of 150 F/g, with energy and power densities of 18.8 Wh/kg and 400 W/kg in a 6M KOH electrolyte¹⁰⁷. Bonso *et al.* composited vanadium oxide nanofibers with graphene for supercapacitors¹²⁷. These devices were tested in an organic electrolyte, and had a resulting capacitance of 226 F/g with energy and power density of 28 Wh/kg and 303 W/kg at 1A/g¹²⁷. While composite electrodes can help to overcome the shortcomings of V₂O₅, research in vanadium nitride (VN) has also received interest for hybrid devices.

Vanadium nitride (VN) has garnered interest as an anode material in energy storage devices due to its high conductivity (1.6x10⁶ S/m) and theoretical capacitance (1350 F/g)¹⁰⁰. Despite the enhanced properties, VN still suffers from poor electrochemical performance in the presence of alkaline or aqueous electrolytes¹⁰⁸. This is due to the oxidation occurring on the surface of VN when in the presence of these types of electrolytes¹⁰³⁻¹⁰⁴. In an aqueous electrolyte (i.e. KOH)

bulk nitride undergoes surface redox processes to form $\text{VN}_x\text{-OH}_y$ ¹⁰⁴. Scheme 5.1 outlines the reaction mechanism in which OH^- ions react with VN surface to form VN_xOH_y ¹⁰³⁻¹⁰⁴.



Scheme 5.1. Reaction mechanism between VN and OH^- in alkaline environment

This can adversely affect the stability of the material over a long cycle duration^{99, 128}. Prior work has shown a retention of ~50% after 1000 cycles when using pure VN as the anode¹²⁸. In order to help overcome the low stability VN, it is composited with a high surface area and conductive carbon material¹⁰³. Through encapsulation of the VN in the carbon, it is possible to develop an electrode material which provides not only high stability but also high energy and power density. This can also be overcome through development of composites which contain mixtures of VN and V_2O_3 . Some have reported that upon testing of pure VN in KOH and K_2SO_4 aqueous electrolytes there was no redox activity present¹²⁹. This study outlines that without the presence of the oxide shell on the VN material, the redox mechanism outlined in Scheme 2.1 cannot occur¹²⁹. Alternatively, without the presence of the highly conductive VN in the material the material would suffer from poor electrical conductivity, as vanadium oxides have conductivities from 10^{-2} - 10^{-6} S/m⁹⁸. These mixtures offer the ability to take advantage of the redox capability of the oxide phase in addition to taking advantage of the conductivity of the VN phase. Development of composites with nitride and oxide mixtures can help to overcome the obstacles presented by electrodes made with pure VN (e.g. cycle lifetime or redox activity). Herein we report a method to synthesize composite vanadium nitride-carbon fiber (VN-CF) mat electrodes for asymmetric supercapacitors. A polyacrylonitrile (PAN) based co-polymer was used as the carbon precursor, and synthesized vanadium oxide nanoflowers were used as the

metal source. Electrospinning was employed to encapsulate the vanadium oxide, at varying concentrations, in the carbon fibers. Vanadium oxide was converted to VN through *in situ* nitridation, followed by oxidation with CO₂. After oxidation with CO₂ composite mats with VN/V₂O₃ mixtures were obtained. The freestanding fiber mats were used as electrodes in asymmetric-hybrid devices, which produced enhanced electrochemical properties.

5.2 Experimental

Materials

Vanadium oxide (V₂O₅, 99%, ACS Grade) crystalline powder was obtained from Acros Organics. Hydrogen peroxide (H₂O₂, 30%, ACS Grade), Isopropanol (IPA, 99%), and N,N-dimethylformamide (DMF, ACS Grade) were purchased from Fisher Scientific. Acrylonitrile (AN, >99%), Itaconic acid (IA, >99%), and 2,2'-Azobis(2-methylpropionitrile) (AIBN, 98%) were purchased from Sigma Aldrich. Cobaltocenium hexafluorophosphate (98%) was obtained from Strem Chemicals. Ionic liquid electrolyte 1-butyl-1-methylpyrrolidinium bis(trifluoromethanesulfonyl)imide (Py₁₄TFSI) was purchased from Iolitec. Lithium bis(trifluoromethanesulfonyl)imide (LiTFSI, 99.5%) was obtained from MTI corporation. All chemicals were used as obtained without any further purification.

Synthesis of Vanadium Oxide Nanoflowers

Vanadium oxide nanoflowers were synthesized by a room temperature sol-gel method. V₂O₅ bulk powder (1.0g) was dispersed in 100mL of deionized water (DI-H₂O), followed by slow addition of 30% hydrogen peroxide (H₂O₂). During the H₂O₂ addition O₂ gas was released, and after complete addition an orange sol was produced. Cobaltocenium hexafluorophosphate (84mg) was dissolved in isopropanol before addition of the organic sol. The sol was then added

to isopropanol (IPA) in a 1:1 v/v ratio and set aside at room temperature for 7 days. Following 7 days a dark green precipitate was collected by vacuum filtration then dried at 225°C in vacuum.

Synthesis of Poly(acrylonitrile-co-itaconic acid) (92/8 wt%) Copolymer

Acrylonitrile based copolymer was synthesized using free-radical polymerization. Acrylonitrile (AN) was first passed through a column of basic alumina to remove the inhibitor. A 250mL round bottom flask was then charged with N₂, followed by addition of 35mL of anhydrous DMF. The DMF was kept under continuous N₂ flow for approximately 15 minutes before addition of monomers. In 35mL of DMF, the initiator AIBN was dissolved followed by addition to monomers AN and IA. The acrylonitrile (AN) and itaconic acid (IA) monomers were reacted at a 92/8 AN/IA weight ratio. This solution was agitated until all materials were dissolved. Monomer solution with initiator was poured into an addition funnel which was used for drop-wise addition. The reaction was kept at 60°C for 48h under continuous nitrogen. After 48h reaction time, the polymer was precipitated using water and ethanol, then dried under vacuum for 48h.

Synthesis Vanadium Nitride-CNF Composite

The V₂O₅ nanoflowers were dispersed in a solution of the 92/8wt% poly(acrylonitrile-co-itaconic acid) (PANIA). V₂O₅ was first probe sonicated in N,N-dimethylformamide (DMF) at three 20s intervals to form a dark green dispersion. Then PANIA (92/8wt%) was dissolved in the dispersions at a concentration of ~30wt% (w.r.t DMF). The polymeric solution was electrospun at a working voltage of 22kV with a needle-to-drum distance of 16 cm. After electrospinning, the mat underwent oxidative stabilization at 215°C for 3.5h using a ramp rate of 2°C/min. The stabilized mat was then carbonized 900°C for 2h with CO₂ activation for 30 minutes.

Electrochemical Testing

Device testing was performed using a coin cell (CR2032) set-up. Electrodes were punched directly from the carbonized mats, using CNFs as the cathode and VN-CNFs as the anode. Ionic liquid 1-butyl-1-methylpyrrolidinium bis(trifluoromethanesulfonyl)imide (Pyr₁₄TFSI) with 0.5M lithium bis(trifluoromethanesulfonyl)imide (LiTFSI) was used as the electrolyte. Coin cells were assembled and pressed in an argon filled glove box. The electrodes were placed on carbon coated aluminum (Toyocarb Inc.) then saturated with electrolyte, an organic cellulose separator was placed between the electrodes. Cyclic voltammetry and galvanostatic charge-discharge (CDC) tests were performed on an Arbin supercapacitor testing station (SCTS). Cyclic voltammetry measurements were taken after equilibration of 20 cycles at a scan rate of 50 mV/sec. The voltage window used for all tests was 3.5V. Galvanostatic charge-discharge (CDC) cycles were measured at a constant current density (1 A/g) up to a voltage of 3.5V.

Characterization

Physical characterization of materials was performed using scanning electron microscopy (SEM), high-resolution transmission electron microscopy (HR-TEM), Raman, and powder x-ray diffraction (XRD). Scanning electron microscopy (SEM) was performed using a Zeiss-LEO Model 1530 variable pressure SEM with an InLens detector. High resolution transmission electron microscopy (HR-TEM) was performed using a JEOL 2100F with a field emission of up to 200kV. Raman spectroscopy was performed on a Yobin-Jvonne with a He-Ne laser at a wavelength of 633nm. XRD measurements were taken using a Rigaku Ultima IV with Cu-K alpha as the radiation source. Chemical characterization was done using x-ray photoelectron spectroscopy (XPS) and thermal gravimetric analysis (TGA). XPS analysis of the samples was

performed using a PHI VersaProbe with Al-K α as the x-ray source. Each sample was charge compensated using a pass energy of 23.5eV. The electron beam was positioned incident with respect to the sample. Surface area and pore size distributions were analyzed on a Micromeritics ASAP 2020 instrument. Brunauer-Emmett-Teller (BET) was used to measure surface area and QSDFT was used for analysis of pore size and distribution. Conductivity was measured using the Van der Pauw four probe method.

5.3 Results and Discussion

Vanadium nitride-carbon fiber (VN-CF) composite electrodes were fabricated using electrospinning, followed by subsequent stabilization and carbonization where VN synthesized by a new method. Synthesized V₂O₅ nanoflowers were used as the precursor, and their morphologies are shown in Fig 5.10. The flowers were made using a new room temperature sol gel method with cobaltocenium as an additive to increase the d-spacing. This method eliminates the need for high temperatures and high-pressure autoclaves often used to produce nanostructured V₂O₅. During the process of carbonization, the vanadium oxide undergoes *in situ* nitridation due to the release of ammonia (NH_{3(g)}) as the PANIA (92/8wt%) pyrolyzes. The *in situ* nitridation is beneficial in that it provides a method to produce VN-CNF composites without the use of physical treatment with NH_{3(g)}.

Powder XRD was performed on activated CF and VN-CF composites. Figure 5.1 shows the patterns of activated CF, 15VN-CF, 30VN-CF, and 45VN-CF. A broad peak at $\sim 25^\circ$ corresponding to the presence of amorphous carbon is present in all samples. The XRD analysis of activated VN-CF composites showed the presence of two vanadium phases, vanadium nitride (VN) and vanadium oxide (V₂O₃). During the process of carbonization vanadium oxide is

converted to vanadium nitride (VN) through *in situ* nitridation with ammonia (NH_{3(g)}). This is due to the release of NH_{3(g)} as the stabilized mat decomposes at higher temperatures. The subsequent process of CO₂ activation oxidizes the VN to the oxide phase of V₂O₃. Scheme 5.2 outlines the balanced chemical reaction between VN and CO₂.



Scheme 5.2. Reaction between VN and CO₂

XRD patterns for the vanadium oxide nanoflower precursor is shown in Figure 5.10 of the supplemental. This pattern shows that there is an increase in the d-spacing of the V₂O₅, which is due to the inclusion of the cobaltocenium complex during synthesis. Additionally, in order to confirm that ammonia is the source of nitridation the nanoflowers were annealed at 900°C for 2h under nitrogen. XRD analysis of the resulting material shows that the phase V₂O₃ was obtained versus VN. This confirmed that VN was obtained through the *in-situ* release of NH₃ during the decomposition of PANIA upon pyrolysis.

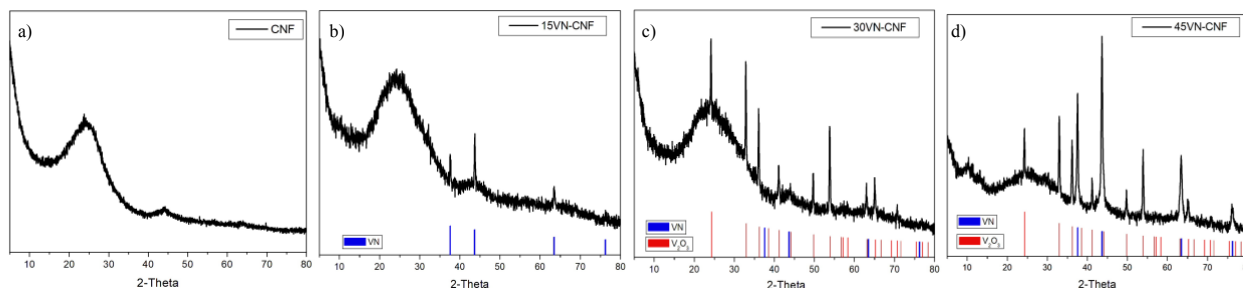


Figure 5.1. XRD patterns of activated (a) CNF, (b) 15VN-CNF, (c) 30VN-CNF, and (d) 45VN-CNF

In order to examine the morphology and structural features of the activated fibers, SEM and high resolution TEM (HRTEM) analysis were performed on CFs and VN-CF composites. SEM imaging of activated CF and VN-CF composites are shown in Figure 5.2. It can be seen that the activated samples consist of a network of nanofibers. The average fiber diameter of the activated

CNF was measured to be $152\pm 40\text{nm}$, where the average diameter for the VN-CNF composites was $106.5\pm 30\text{nm}$. SEM imaging of V_2O_5 nanoflowers is shown in Figure 5.10 in the supplemental section. The nanoflowers consist of a network of smaller fibers and rods.

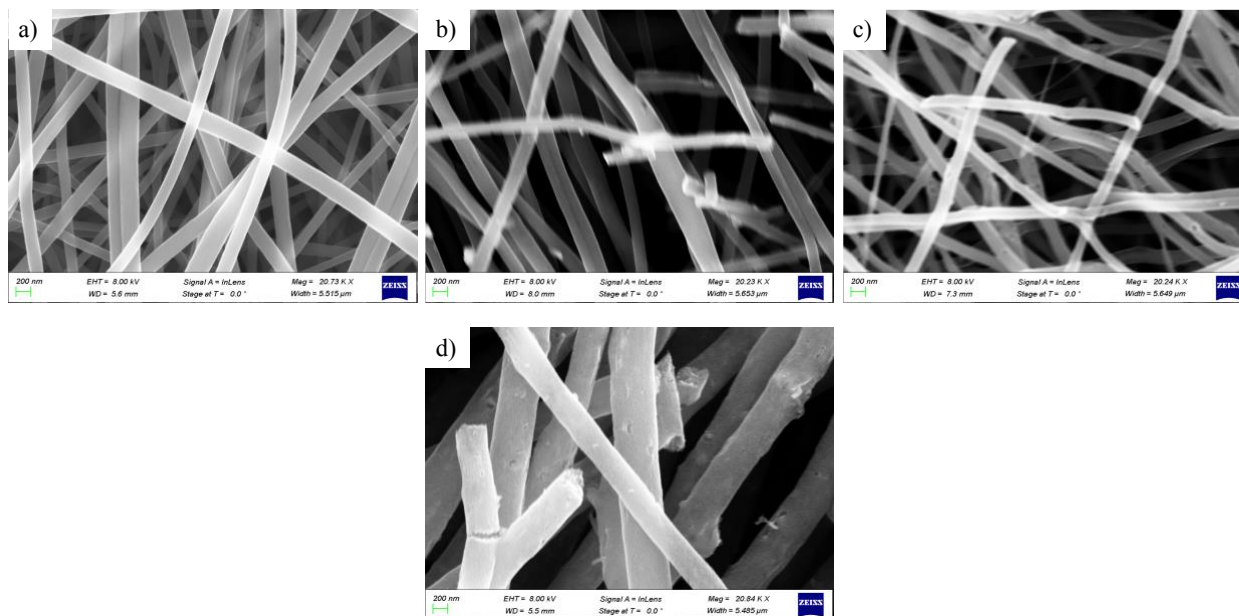


Figure 5.2. SEM images of (a) CNF, (b) 15VN-CNF, (c) 30VN-CNF, and (d) 45VN-CNF. HR-TEM imaging was used to analyze the structural features of the activated CF and VN-CF composites. This showed whether the vanadium was encapsulated within the fibers or if it had dispersed towards the outside during carbonization and subsequent activation. Figure 5.3 displays the TEM imaging of activated CNF and VN-CNF composites. In both the VN-CNF composites vanadium particles were encapsulated inside the CNFs. TEM imaging of V_2O_5 nanoflowers are shown in Figure 5.10 (b-c) of the supplemental. Images of as synthesized nanoflowers indicate that the individual petals consist of smaller nanorods. Imaging of the probe sonicated sample showed that the nanoflowers broke up into small bundles of nanorods.

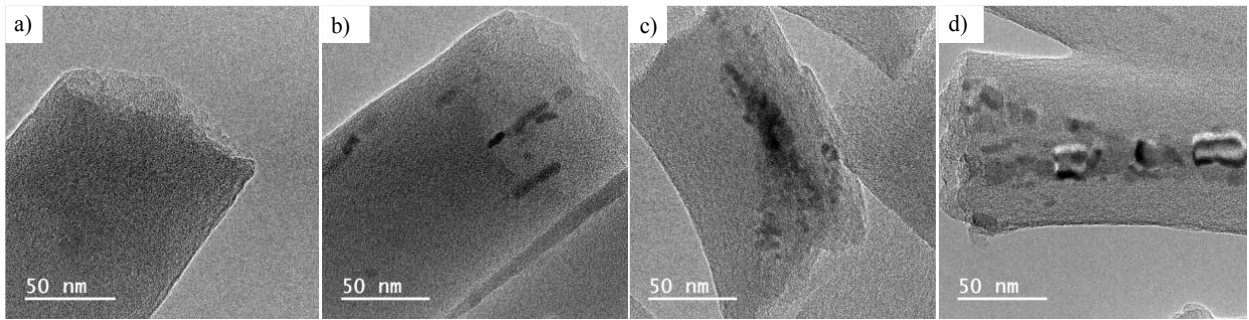


Figure 5.3 TEM images of (a) CNF, (b) 15VN-CNF, (c) 30VN-CNF, and (d) 45VN-CNF.

5.3.1 XPS Analysis for determination of Vanadium Species in CF samples

To determine the presence of vanadium species in the composite electrodes, *ex situ* XPS analysis was performed. This was also performed on the V_2O_5 nanoflowers which were used at the vanadium precursor. XPS analysis of the nanoflowers is shown in Figure 5.12 in the Supplemental section. The analysis confirmed the presence of only oxide species in the sample, and the C-O species present are from the carbon tape which was used to load the sample. Figure 5.4 displays the C1s, O1s, N1s, and V2p3 spectra collected for the samples after activation. For the CF sample, a π - π^* transition was observed in the C1s spectra (Figure 5.4a) at 291 eV. This is attributed to the delocalization of electrons across the carbon backbone. The O1s spectra (Figure 5.4b) had peaks at 537.7 and 531.8 eV corresponding to organic oxygen groups, such as C=O and O(=C)=C. Peaks at 402.6, 400.5, and 398 eV in the N1s spectra (Figure 5.4c) of CF correspond to N-OC, NH_x -C, and N=C. There was also a peak at 405.7 eV which corresponds to a π - π^* transition peak, which is indication that nitrogen is present in the carbon backbone.

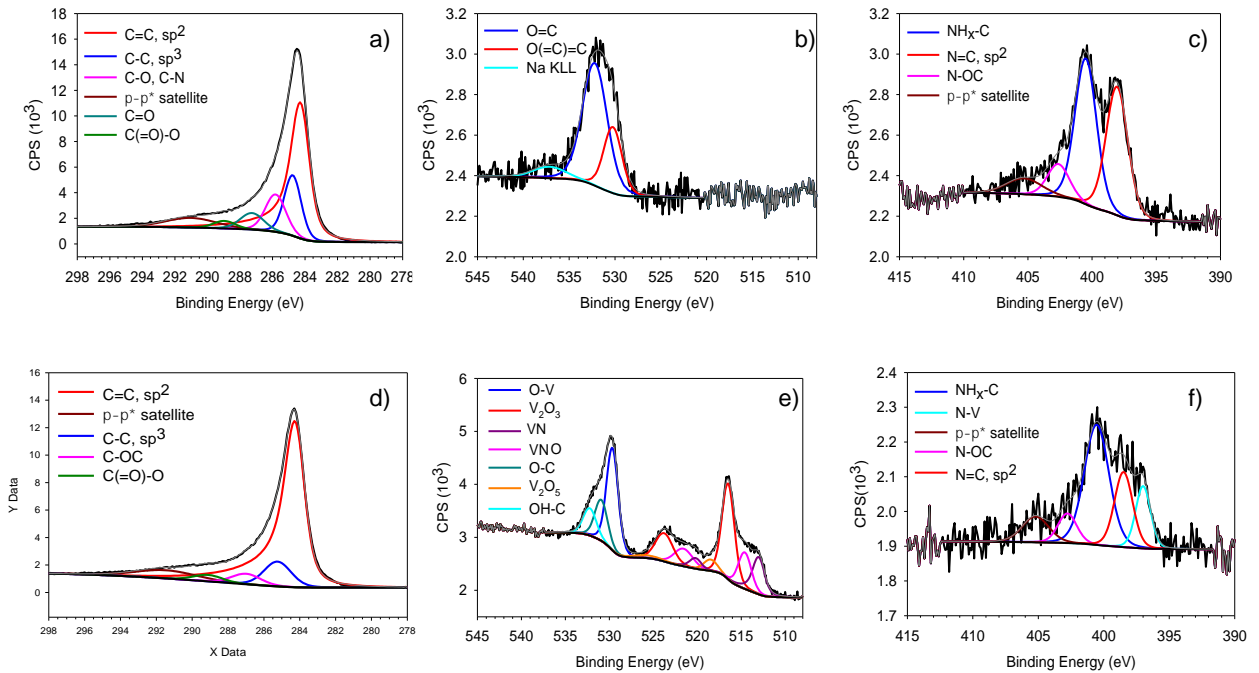


Figure 5.4. XPS Spectra of (a) C1s, (b) O1s, and (c) N1s for activated CNF and (d) C1s, (e) V2p, and (f) N1s for activated 45VN-CNF

The 45VN-CF XPS spectra are displayed in Figure 5.5 d-f. Due to the presence of vanadium oxide in 45VN-CF, the O1s spectra was collected with the V2p spectra. The C1s spectra for this sample had peaks at 289, 286.5, 284.7, and 284.2eV which correspond to C(=O)-O, C-OC, C-C, and C=C, respectively. There was also a peak at 291.3eV corresponding to the π - π^* transition. This transition is due to delocalization of electrons across aromatic rings and can give some indication to the conductivity of the sample. Peaks at 533 and 531.2eV in the O1s spectra correspond to the binding energies of C-O and C=O for organic carbonyls. The V2p_{3/2} spectra showed peaks at binding energies at 520.2 and 513.0eV which corresponds to the vanadium of VN. A peak present at 514.6eV corresponds to that of VNO. Additional peaks present at 516.5, 518.2, and 529.6eV are appointed to the vanadium of V₂O₃. A peak centered at 397.2eV in the N1s spectra is associated with the N-V bonding in VN, the additional peaks centered at 403.8,

400.7, and 398.5eV are associated with amides, amines, and aromatic nitrogen. There was also a peak at ~405eV, similar to CF, which is indicative of the π - π^* transition due to aromatic C=N (sp^2) bonding in the material.

5.3.1 Raman Characterization and Analysis

Raman analysis helps to determine the graphitic nature of each sample. Figure 5.5 displays the Raman spectra collected for all samples. Two peaks are present which corresponds to the carbon's amorphous and graphitic nature. D-band relates to the disordered or amorphous sp^3 carbon, and G-band correlates to the graphitic sp^2 carbon. The degree of graphitization can be determined by taking the relative intensity ratios of the D and G bands (I_D/I_G). A lower ratio the more graphitic content present in the material. In order to obtain the relative D and G band intensities each spectrum was deconvoluted using Gaussian-Lorentzian fitting parameters on LabSpec 6 software. Table 5.1 lists the I_D/I_G ratios for each CF and VN-CF sample. CF sample had a ratio of 1.17, with the ratios increasing after incorporation of the metal. Ratios went from 1.21, 1.16, to 1.21 for 15VN-CF, 30VN-CF, and 45VN-CF respectively. After fitting, an additional two peaks show corresponding to D' and D''. The D' band relates to the sp^2 - sp^3 bonds where the D'' corresponds to interstitial defects present within the graphitic lattice of the carbon. Figure 5.5 depicts the Raman spectra collected for each sample.

Table 5.1. I_D/I_G Ratios of Activated VN-CNF Samples

Sample	I_D/I_G Ratio	Conductivity (S/m)
CNF	1.17	13
15VN-CNF	1.21	68
30VN-CNF	1.16	91
45VN-CNF	1.21	155

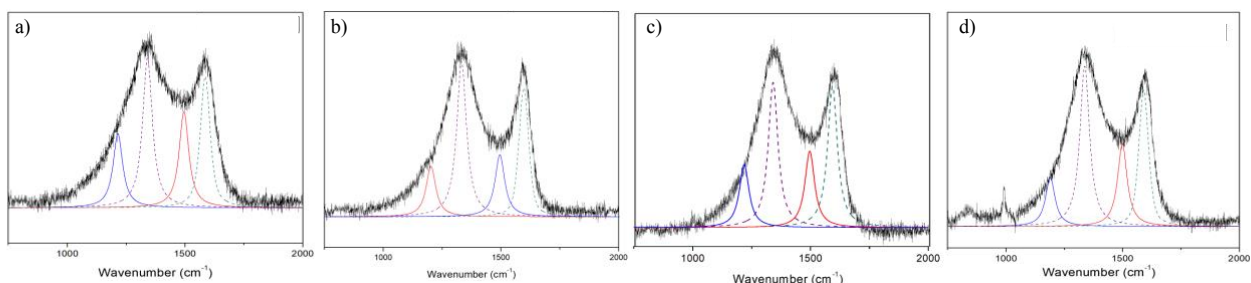


Figure 5.5. Raman spectra of (a) CNF, (b) 15VN-CNF, (c) 30VN-CNF, and (d) 45VN-CNF

5.3.2 Surface Area and Pore Size Analysis

Pore size distribution analysis of the samples are displayed in Figure 5.6. Table 5.2 outlines the surface areas of activated CNF and VN-CNF samples. Surface area was measured to be 250 m²/g (15VN-CNF), 708 m²/g (30VN-CNF), and 350 m²/g (45VN-CNF). There is an increase in surface area as vanadium concentration increases with the exception of 45VN-CNF sample. The decrease observed is due to the increasing concentration of vanadium present in the sample. At higher concentrations there is a greater possibility for the metal to fill a higher percent of the pores in the fibers. The surface areas observed for these materials are higher versus prior reports of VN-carbon composite materials^{108, 110, 130}. While all samples displayed a significant amount of microporosity (<10 nm), each also indicates the presence of mesopores (>10 nm).

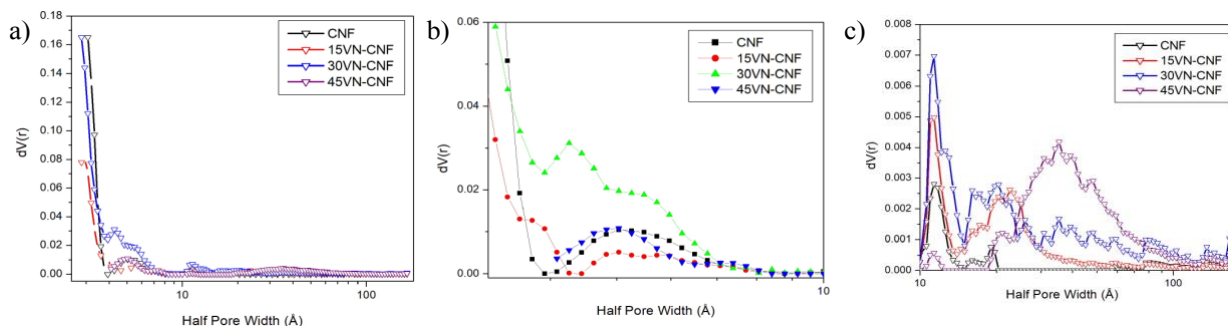


Figure 5.6. (a) Pore size distribution, (b) Micropore distribution, and (c) Mesopore of activated VN-CNF materials

Table 5.2. BET surface area of activated VN-CNF samples

Sample	Surface Area
CNF	421 m ² /g
15VN-CNF	250 m ² /g
30VN-CNF	750 m ² /g
45VN-CNF	450 m ² /g

5.3.3. Electrochemical Characterization

Electrochemical analysis of the VN-CNF composites was performed using a two-electrode coin-cell set-up. Activated CNFs served as the cathode and the activated VN-CNF composite served as the anode in the device. Both electrodes were saturated with 0.5M LiTFSI in Pyr₁₄TFSI ionic liquid electrolyte. Figure 5.7 displays the resulting CV curves obtained for each sample. The cyclic voltammograms observed for CNF displayed a semi-rectangular shape, where those observed for VN-CNF samples showed the presence of redox activity. Table 5.3 outlines corresponding capacitance values, in addition to energy and power densities for each device. At a scan rate of 10 mV/sec CNF sample showed a C_{sp} of 88 F/g, which increased with increasing concentration of vanadium. The 45VN-CNF gave the highest capacitance at 234 F/g, followed by 30VN-CNF (154 F/g) then 15VN-CNF (95 F/g). In addition to achieving the highest capacitance, 45VN-CNF achieved the highest energy density of 67.1 Wh/kg with a power density of 1701 W/kg at a current density of 1 A/g. Figure 5.8 displays the charge discharge curves for activated CNF and VN-CNF composites and the Ragone plot.

Table 5.3. Electrochemical Results for activated CNF and VN-CNF samples

Sample	Capacitance (F/g) (10 mV/sec)	Energy Density (Wh/kg) (1 A/g)	Power Density (W/kg) (1 A/g)
CNF	88	36.8	1424
15VN-CNF	95	41.6	1576
30VN-CNF	154	46.5	1609
45VN-CNF	234	67.1	1701

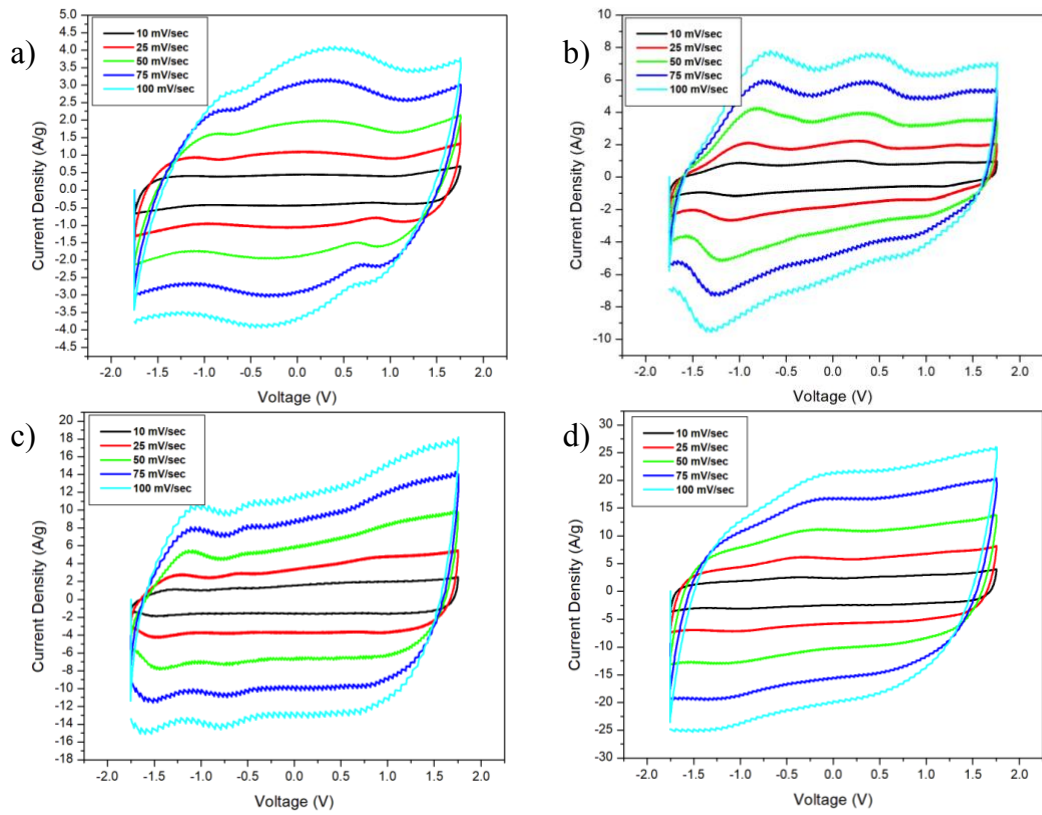


Figure 5.7. Cyclic voltammetry (CV) results for (a) CNF, (b) 15VN-CNF, (c) 30VN-CNF, and (d) 45VN-CNF

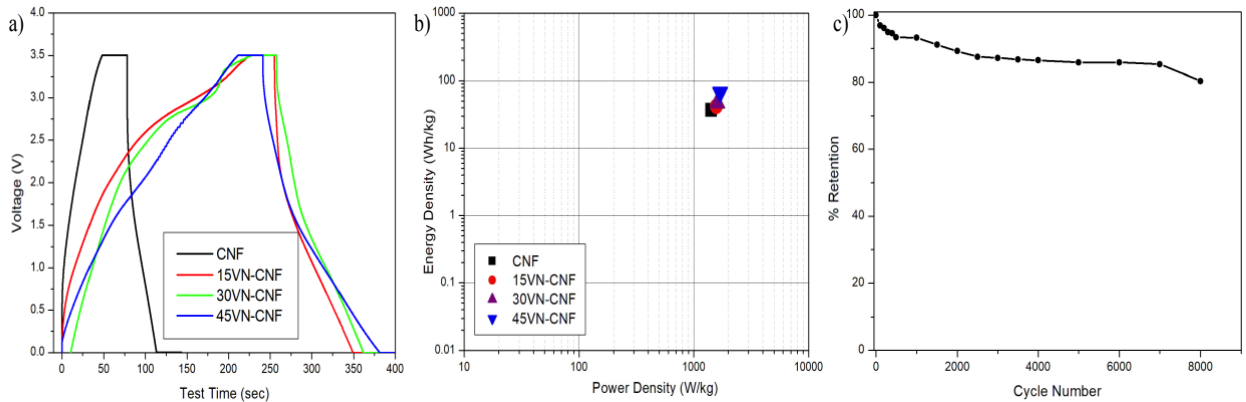


Figure 5.8. (a) CDC curves of CNF and VN-CNF samples (b) Ragone Plot and (c) Cycle Test of 45VN-CNF after 8000 cycles

A cycle test done with the activated 45VN-CNF sample shows that capacitance was stabilized at ~85% and sustained until 7,000 cycles and then decreased to ~80% level. The decrease may be due to the imperfect encapsulation of the VN within the CNF matrix. Additionally, if there is any residual water present in the sample then the stability of the electrode can also be deteriorated. Those may be the reasons for the observed decrease in retention observed in the cycle test. Better encapsulation and moisture control with characterization of the tested electrode will be the future study to find if the cycle test performance can be improved. Once the performance improvement is achieved, this is a promising electrode material for use in hybrid-asymmetric devices.

5.3.4 Charge Contribution and Kinetics Analysis of Composites

In order to understand the charge storage mechanism for these materials, kinetics and charge contributions were analyzed. Trasatti *et al.* reported a method in which charge contributions can be separated¹³¹⁻¹³². He reported that graphing the linear relationship between the inverse scan rate ($v^{1/2}$) and total charge stored (C_t), the percent contributions from surface and diffusive charges can be separated¹³¹⁻¹³². The total volumetric charge, Q_t , can be separated in to two components: surface controlled (Q_s) and diffusion controlled (Q_d). All three of these variables can be related in equation 5.1.

$$\text{Eqn 5.1. } Q_t = Q_s + Q_d$$

Graphing the total stored charge versus the reciprocal of the square root of the scan rate of each sample. Q_s and Q_d can be extrapolated from the equation of the line. Extrapolation of each variable was possible by the equation of the line attained from each plot where y-intercent (b) is the Q_s value and $Cv^{-1/2}$ (mx) is the Q_d , as outlined in Equation 5.2.

$$\text{Eqn 5.2. } y = Q_s + Cv^{-1/2}$$

Figure 5.9 shows the percent contributions from Q_s and Q_d obtained for each composite sample at five different scan rates. At the lowest loading of vanadium (15VN-CNF) the charge contribution was dominated by surface reactions, due to bulk surface redox reactions occurring on the surface of the VN. The highest loading of VN (45VN-CNF) showed the charge contribution was dominated by Q_s at all scan rates (10-100 mV/sec).

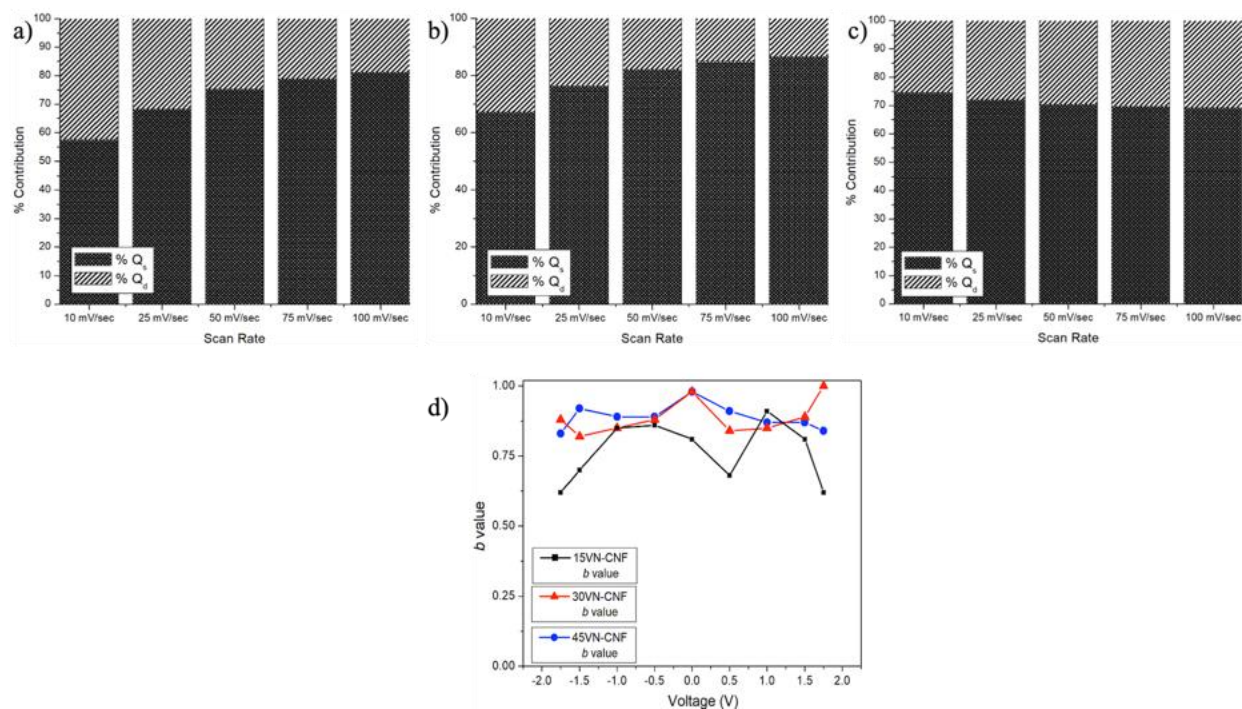


Figure 5.9. Separation of charge contribution for (a) 15VN-CNF, (b) 30VN-CNF, and (c) 45VN-CNF and (d) b values for VN-CNF composites

The charge storage mechanism observed for each sample can be obtained by establishing the b value for each sample. Dunn *et al.* reported that based on the value of b one can determine if the material has pseudocapacitive/capacitive or intercalative properties^{95, 133-134}. According to his work, when b is equal to 0.5 the mechanism of charge storage is primarily from intercalation and when b is equal to 1.0 it is pseudocapacitive/capacitive (not diffusion limited)^{95, 101, 133-134}. Intercalation charge storage ($b = 0.5$) primarily involves slow ion diffusion and faradaic charges.

Capacitive/pseudocapacitive charge storage ($b = 1.0$) involves double-layer, fast surface redox reactions, or a combination of the two. This makes it possible to distinguish if the device exhibits intercalative, pseudocapacitive, double-layer type behavior, or a combination of pseudocapacitive/EDLC. The charge storage mechanism can be determined by equation 5.3, where i corresponds to the peak current, v is the scan rate, and a and b are constants.

$$\text{Eqn 5.3. } i = av^b$$

The b value is determined by plotting $\log v$ versus $\log i$ and analyzing the linear relationship between the two. The slope of this line corresponds to the b value. Figure 5.9d plots the b values calculated at different potentials for each different VN-CNF sample. At the lowest loading of vanadium (15VN-CNF) the b value of 0.6 indicative of a slow intercalative storage mechanism, where 30VN-CNF and 45VN-CNF have values of 0.8. This indicates that they have a pseudocapacitive/EDLC charge storage mechanism and have a high rate capability^{95, 101}. Two mechanisms contribute to 30VN-CNF and 45VN-CNF, (i) double layer interactions and (ii) fast redox reactions occurring on the surface on the VN.

5.4 Conclusion

Hybrid, asymmetric devices were successfully assembled using composites of activated CNFs and VN-CNFs. Ionic liquid Pyr14 TFSI with LiTFSI was used as the electrolyte in these devices. Cyclic voltammetry results of 45VN-CF exhibited a high specific capacitance of 234 F/g with a maximum energy density of 67.1 Wh/kg and power density of 1644 W/kg at 1 A/g. These results were an improvement over CNF, 36.8 Wh/kg and 1424 W/kg (1 A/g), respectively, which confirms that incorporation of redox-active vanadium in CNF can help increase performance. At the highest loading of vanadium, the composite electrode had a 75% contribution from surface

capacitive charge, which corresponds to its b value of ~ 0.8 indicative of a pseudocapacitive/capacitive based storage mechanism. Cycle test performed with activated 45VN-CNF composite shows an 80% retention after 8000 cycles. It is possible to increase the retention through better encapsulation of VN inside CNF. Postmortem characterization of the tested electrode will be the future study to find solutions if the performance can be improved with enhanced cycle life. Once the performance improvement is achieved, this can be a promising electrode material for use in hybrid-asymmetric devices.

5.5 Appendix – Supporting Information

5.5.1 Characterization of as-synthesized and annealed V_2O_5 nanoflowers used as precursors in VN-CF composites.

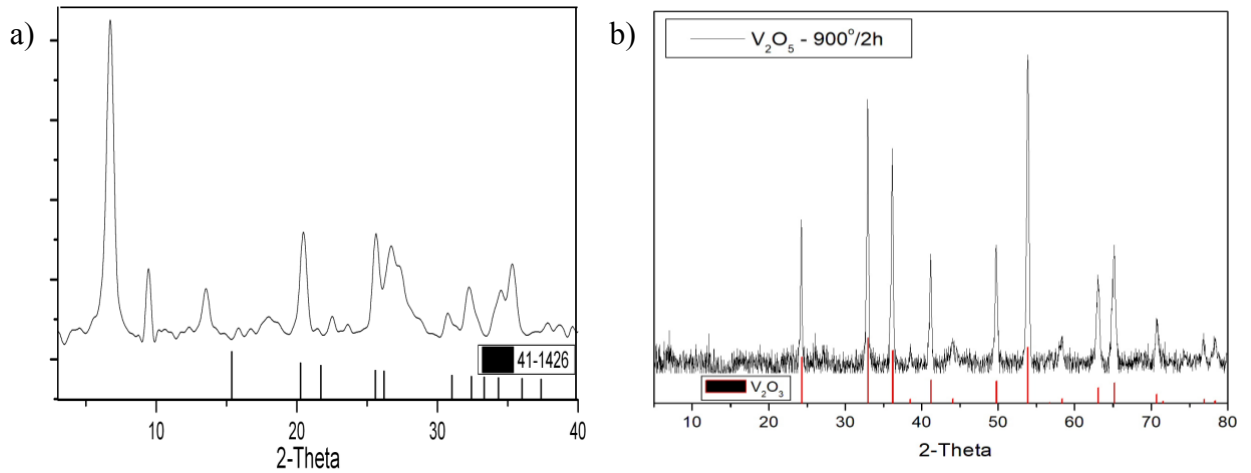


Figure 5.10. XRD of (a) as-synthesized V_2O_5 nanoflowers and (b) V_2O_5 nanoflowers at 900°C under N_2

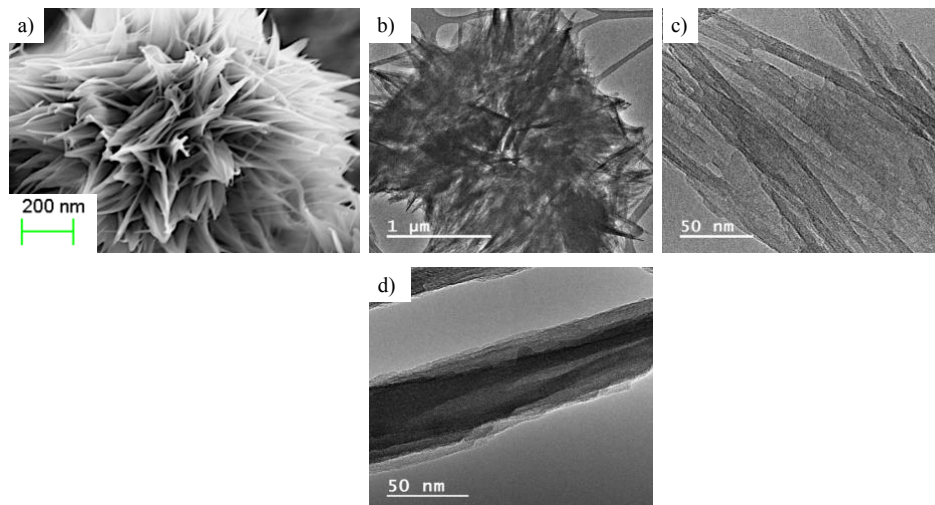


Figure 5.11. (a) SEM image of V_2O_5 nanoflowers and TEM imaging (b) as-synthesized V_2O_5 nanoflowers and (c) probe-sonicated V_2O_5 nanoflowers

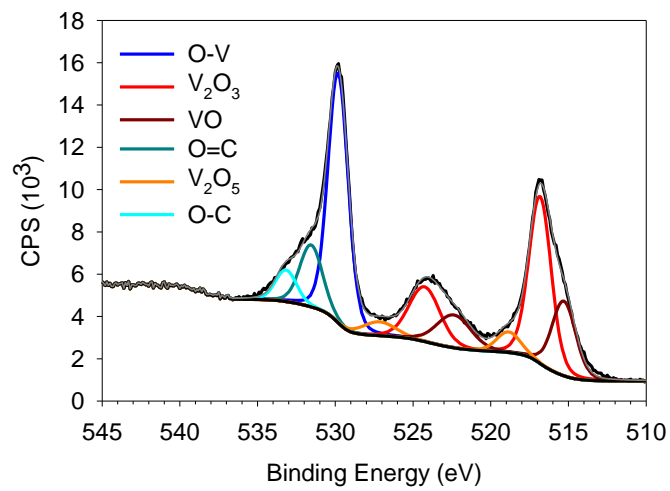


Figure 5.12. XPS of V₂O₅ nanoflowers

REFERENCES

1. Peplow, M., The quest for supercarbon. *Nature* **2013**, *503* (7476), 327-329.
2. Antonietti, M.; Mllen, K., Chemical Synthesis and Applications of Graphene and Carbon Materials. John Wiley & Sons (US),: Place of publication not identified, 2017; p. 1 online resource (272 pages).
3. Ghaemi, F.; Abdullah, L. C.; Tahir, P. M.; Yunus, R., Synthesis of Different Layers of Graphene on Stainless Steel Using the CVD Method. *Nanoscale Res Lett* **2016**, *11* (1), 506.
4. Vishwakarma, R.; Zhu, R.; Abuelwafa, A. A.; Mabuchi, Y.; Adhikari, S.; Ichimura, S.; Soga, T.; Umeno, M., Direct Synthesis of Large-Area Graphene on Insulating Substrates at Low Temperature using Microwave Plasma CVD. *ACS Omega* **2019**, *4* (6), 11263-11270.
5. Ramakrishnan, S.; Jelmy, E. J.; Senthilkumar, R.; Rangarajan, M.; Kothurkar, N. K., One-Step RF-CVD Method for the Synthesis of Graphene Decorated with Metal and Metal Oxide Nanoparticles. *J Nanosci Nanotechnol* **2018**, *18* (2), 1089-1096.
6. Zhang, C.; Man, B. Y.; Yang, C.; Jiang, S. Z.; Liu, M.; Chen, C. S.; Xu, S. C.; Sun, Z. C.; Gao, X. G.; Chen, X. J., Facile synthesis of graphene on dielectric surfaces using a two-temperature reactor CVD system. *Nanotechnology* **2013**, *24* (39), 395603.
7. Li, Y.; Li, Z.; Li, Q.; Tian, M.; Li, C.; Sun, L.; Wang, J.; Zhao, X.; Xu, S.; Yu, F., Direct Synthesis of Graphene Dendrites on SiO₂/Si Substrates by Chemical Vapor Deposition. *Nanoscale Res Lett* **2020**, *15* (1), 16.
8. Jayasena, B.; Reddy, C. D.; Subbiah, S., Separation, folding and shearing of graphene layers during wedge-based mechanical exfoliation. *Nanotechnology* **2013**, *24* (20), 205301.
9. Ren, S.; Meng, L.; Ma, W.; Lin, S.; Yang, W.; Lan, J.; Jia, X.; Cai, Q.; Yang, X., Enhancing overall properties of epoxy-based composites using polydopamine-coated edge-carboxylated graphene prepared via one-step high-pressure ball milling. *Phys Chem Chem Phys* **2019**, *21* (39), 21726-21737.
10. Pang, S.; Englert, J. M.; Tsao, H. N.; Hernandez, Y.; Hirsch, A.; Feng, X.; Mullen, K., Extrinsic corrugation-assisted mechanical exfoliation of monolayer graphene. *Adv Mater* **2010**, *22* (47), 5374-7.
11. Li, X.; Shen, J.; Wu, C.; Wu, K., Ball-Mill-Exfoliated Graphene: Tunable Electrochemistry and Phenol Sensing. *Small* **2019**, *15* (48), e1805567.
12. Geim, A. K.; Novoselov, K. S., The rise of graphene. *Nat Mater* **2007**, *6* (3), 183-91.

13. Novoselov, K. S.; Geim, A. K.; Morozov, S. V.; Jiang, D.; Zhang, Y.; Dubonos, S. V.; Grigorieva, I. V.; Firsov, A. A., Electric field effect in atomically thin carbon films. *Science* **2004**, *306* (5696), 666-9.
14. Jeon, I. Y.; Bae, S. Y.; Seo, J. M.; Baek, J. B., Scalable Production of Edge-Functionalized Graphene Nanoplatelets via Mechanochemical Ball-Milling. *Adv Funct Mater* **2015**, *25* (45), 6961-6975.
15. Jeon, I. Y.; Choi, H. J.; Jung, S. M.; Seo, J. M.; Kim, M. J.; Dai, L.; Baek, J. B., Large-scale production of edge-selectively functionalized graphene nanoplatelets via ball milling and their use as metal-free electrocatalysts for oxygen reduction reaction. *J Am Chem Soc* **2013**, *135* (4), 1386-93.
16. Chua, C. K.; Sofer, Z.; Khezri, B.; Webster, R. D.; Pumera, M., Ball-milled sulfur-doped graphene materials contain metallic impurities originating from ball-milling apparatus: their influence on the catalytic properties. *Phys Chem Chem Phys* **2016**, *18* (27), 17875-80.
17. Xu, J.; Jeon, I. Y.; Seo, J. M.; Dou, S.; Dai, L.; Baek, J. B., Edge-selectively halogenated graphene nanoplatelets (XGnPs, X = Cl, Br, or I) prepared by ball-milling and used as anode materials for lithium-ion batteries. *Adv Mater* **2014**, *26* (43), 7317-23.
18. Feng, W.; Long, P.; Feng, Y.; Li, Y., Two-Dimensional Fluorinated Graphene: Synthesis, Structures, Properties and Applications. *Advanced Science* **2016**, *3* (7), 1500413.
19. Chen, J.; Yao, B.; Li, C.; Shi, G., An improved Hummers method for eco-friendly synthesis of graphene oxide. *Carbon* **2013**, *64*, 225-229.
20. Chronopoulos, D. D.; Bakandritsos, A.; Pykal, M.; Zboril, R.; Otyepka, M., Chemistry, properties, and applications of fluorographene. *Appl Mater Today* **2017**, *9*, 60-70.
21. Chen, J.; Li, Y.; Huang, L.; Li, C.; Shi, G., High-yield preparation of graphene oxide from small graphite flakes via an improved Hummers method with a simple purification process. *Carbon* **2015**, *81*, 826-834.
22. Shahriary, L.; Athawale, A. A., Graphene oxide synthesized by using modified hummers approach. *Int. J. Renew. Energy Environ. Eng* **2014**.
23. Guerrero-Contreras, J.; Caballero-Briones, F., Graphene oxide powders with different oxidation degree, prepared by synthesis variations of the Hummers method. *Materials Chemistry and Physics* **2015**, *153*, 209-220.
24. Marcano, D. C.; Kosynkin, D. V.; Berlin, J. M.; Sinitskii, A.; Sun, Z. Z.; Slesarev, A.; Alemany, L. B.; Lu, W.; Tour, J. M., Improved Synthesis of Graphene Oxide. *Acs Nano* **2010**, *4* (8), 4806-4814.

25. Tang, L. B.; Li, X. M.; Ji, R. B.; Teng, K. S.; Tai, G.; Ye, J.; Wei, C. S.; Lau, S. P., Bottom-up synthesis of large-scale graphene oxide nanosheets. *Journal of Materials Chemistry* **2012**, *22* (12), 5676-5683.
26. Alzate-Carvajal, N.; Basiuk, E. V.; Meza-Laguna, V.; Puente-Lee, I.; Farias, M. H.; Bogdanchikova, N.; Basiuk, V. A., Solvent-free one-step covalent functionalization of graphene oxide and nanodiamond with amines. *Rsc Advances* **2016**, *6* (114), 113596-113610.
27. Bon, S. B.; Valentini, L.; Verdejo, R.; Fierro, J. L. G.; Peponi, L.; Lopez-Manchado, M. A.; Kenny, J. M., Plasma Fluorination of Chemically Derived Graphene Sheets and Subsequent Modification With Butylamine. *Chem Mater* **2009**, *21* (14), 3433-3438.
28. Chakraborty, S.; Saha, S.; Dhanak, V. R.; Biswas, K.; Barbezat, M.; Terrasi, G. P.; Chakraborty, A. K., High yield synthesis of amine functionalized graphene oxide and its surface properties. *Rsc Advances* **2016**, *6* (72), 67916-67924.
29. Park, M. S.; Kim, K. H.; Kim, M. J.; Lee, Y. S., NH₃ gas sensing properties of a gas sensor based on fluorinated graphene oxide. *Colloid Surface A* **2016**, *490*, 104-109.
30. Aguilar-Bolados, H.; Vargas-Astudillo, D.; Yazdani-Pedram, M.; Acosta-Villavicencio, G.; Fuentealba, P.; Contreras-Cid, A.; Verdejo, R.; Lopez-Manchado, M. A., Facile and Scalable One-Step Method for Amination of Graphene Using Leuckart Reaction. *Chem Mater* **2017**, *29* (16), 6698-6705.
31. Ghaleb, Z. A.; Mariatti, M.; Ariff, Z. M., Effect of Amino-functionalized on Tensile and Electrical Properties of Graphene Nanopowder Filled Epoxy Thin Film Nanocomposite. *J Polym Mater* **2016**, *33* (1), 155-164.
32. Navaee, A.; Salimi, A., Efficient amine functionalization of graphene oxide through the Bucherer reaction: an extraordinary metal-free electrocatalyst for the oxygen reduction reaction. *Rsc Advances* **2015**, *5* (74), 59874-59880.
33. Arbuzov, A. A.; Muradyan, V. E.; Tarasov, B. P.; Sokolov, E. A., Preparation of Amino-Functionalized Graphene Sheets and their Conductive Properties. *Preparation of Amino-Functionalized Graphene Sheets and their Conductive Properties* **2013**.
34. Ramezanzadeh, B.; Niroumandrad, S.; Ahmadi, A.; Mahdavian, M.; Moghadam, M. H. M., Enhancement of barrier and corrosion protection performance of an epoxy coating through wet transfer of amino functionalized graphene oxide. *Corros Sci* **2016**, *103*, 283-304.
35. Tetsuka, H.; Nagoya, A.; Asahi, R., Highly luminescent flexible amino-functionalized graphene quantum dots@ cellulose nanofiber– clay hybrids for white-light emitting diodes. *Journal of Materials Chemistry C* **2015**, *3* (15), 3536-3541.

36. Shanmugaraj, A. M.; Yoon, J. H.; Yang, W. J.; Ryu, S. H., Synthesis, characterization, and surface wettability properties of amine functionalized graphene oxide films with varying amine chain lengths. *Journal of Colloid and Interface Science* **2013**, *401*, 148-154.
37. Bi, X.; Li, Y.; Qiu, Z.; Liu, C.; Zhou, T.; Zhuo, S.; Zhou, J., Fluorinated Graphene Prepared by Direct Fluorination of N, O-Doped Graphene Aerogel at Different Temperatures for Lithium Primary Batteries. *Materials (Basel)* **2018**, *11* (7).
38. Mazánek, V.; Jankovský, O.; Luxa, J.; Sedmidubský, D.; Janoušek, Z.; Šembera, F.; Mikulics, M.; Sofer, Z., Tuning of fluorine content in graphene: towards large-scale production of stoichiometric fluorographene. *Nanoscale* **2015**, *7* (32), 13646-13655.
39. Mathkar, A.; Narayanan, T. N.; Alemany, L. B.; Cox, P.; Nguyen, P.; Gao, G.; Chang, P.; Romero-Aburto, R.; Mani, S. A.; Ajayan, P. M., Synthesis of Fluorinated Graphene Oxide and its Amphiphobic Properties. *Particle & Particle Systems Characterization* **2013**, *30* (3), 266-272.
40. Yang, Z. Q.; Wang, L. D.; Sun, W.; Li, S. J.; Zhu, T. Z.; Liu, W.; Liu, G. C., Superhydrophobic epoxy coating modified by fluorographene used for anti-corrosion and self-cleaning. *Applied Surface Science* **2017**, *401*, 146-155.
41. Yang, Z. Q.; Sun, W.; Wang, L. D.; Li, S. J.; Zhu, T. Z.; Liu, G. C., Liquid-phase exfoliated fluorographene as a two dimensional coating filler for enhanced corrosion protection performance. *Corros Sci* **2016**, *103*, 312-318.
42. Prasai, D.; Tuberquia, J. C.; Harl, R. R.; Jennings, G. K.; Bolotin, K. I., Graphene: Corrosion-Inhibiting Coating. *Acs Nano* **2012**, *6* (2), 1102-1108.
43. Alam, J.; Ryu, S. H.; Shanmugaraj, A. M., Influence of Hexamethylenediamine Functionalized Graphene Oxide on Structural Characteristics and Properties of Epoxy Nanocomposites. *Sci Adv Mater* **2015**, *7* (5), 993-1001.
44. Wang, C. Y.; Lan, Y. F.; Yu, W. T.; Li, X.; Qian, Y.; Liu, H. S., Preparation of amino-functionalized graphene oxide/polyimide composite films with improved mechanical, thermal and hydrophobic properties. *Applied Surface Science* **2016**, *362*, 11-19.
45. Lee, J. H.; Park, N.; Kim, B. G.; Jung, D. S.; Im, K.; Hur, J.; Choi, J. W., Restacking-Inhibited 3D Reduced Graphene Oxide for High Performance Supercapacitor Electrodes. *Acs Nano* **2013**, *7* (10), 9366-9374.
46. Li, J. T.; Ostling, M., Prevention of Graphene Restacking for Performance Boost of Supercapacitors-A Review. *Crystals* **2013**, *3* (1), 163-190.
47. Abbas, R.; Elkhoshkhany, N.; Hefnawy, A.; Ebrahim, S.; Rahal, A., High Stability Performance of Superhydrophobic Modified Fluorinated Graphene Films on Copper Alloy Substrates. *Adv Mater Sci Eng* **2017**.

48. Raman, R. K. S.; Tiwari, A., Graphene: The Thinnest Known Coating for Corrosion Protection. *Jom-Us* **2014**, *66* (4), 637-642.
49. Novoselov, K. S.; Fal'ko, V. I.; Colombo, L.; Gellert, P. R.; Schwab, M. G.; Kim, K., A roadmap for graphene. *Nature* **2012**, *490* (7419), 192-200.
50. Chen, C.; Qiu, S. H.; Cui, M. J.; Qin, S. L.; Yan, G. P.; Zhao, H. C.; Wang, L. P.; Xue, Q. J., Achieving high performance corrosion and wear resistant epoxy coatings via incorporation of noncovalent functionalized graphene. *Carbon* **2017**, *114*, 356-366.
51. Kim, J.; Carlin, J. M.; Smith, S. A.; Yin, J.; Joo, Y. L., Thermal restacking of graphene structure to improve lithium-air battery cyclability. *Electrochemistry Communications* **2016**, *70*, 43-46.
52. Chen, Y.; Zhang, X. O.; Zhang, D. C.; Yu, P.; Ma, Y. W., High performance supercapacitors based on reduced graphene oxide in aqueous and ionic liquid electrolytes. *Carbon* **2011**, *49* (2), 573-580.
53. Tan, B.; Thomas, N. L., A review of the water barrier properties of polymer/clay and polymer/graphene nanocomposites. *J Membrane Sci* **2016**, *514*, 595-612.
54. Nine, M. J.; Cole, M. A.; Tran, D. N. H.; Losic, D., Graphene: a multipurpose material for protective coatings. *Journal of Materials Chemistry A* **2015**, *3* (24), 12580-12602.
55. Ramezanzadeh, B.; Ghasemi, E.; Mahdavian, M.; Changizi, E.; Moghadam, M. H. M., Covalently-grafted graphene oxide nanosheets to improve barrier and corrosion protection properties of polyurethane coatings. *Carbon* **2015**, *93*, 555-573.
56. Chaudhry, A. U.; Mittal, V.; Mishra, B., Inhibition and promotion of electrochemical reactions by graphene in organic coatings. *Rsc Advances* **2015**, *5* (98), 80365-80368.
57. Mo, M.; Zhao, W.; Chen, Z.; Yu, Q.; Zeng, Z.; Wu, X.; Xue, Q., Excellent tribological and anti-corrosion performance of polyurethane composite coatings reinforced with functionalized graphene and graphene oxide nanosheets. *RSC Advances* **2015**, *5* (70), 56486-56497.
58. Konios, D.; Stylianakis, M. M.; Stratakis, E.; Kymakis, E., Dispersion behaviour of graphene oxide and reduced graphene oxide. *Journal of colloid and interface science* **2014**, *430*, 108-112.
59. Zhou, B. M.; Qian, X. M.; Li, M. M.; Ma, J. L.; Liu, L. S.; Hu, C. S.; Xu, Z. W.; Jiao, X. N., Tailoring the chemical composition and dispersion behavior of fluorinated graphene oxide via CF₄ plasma. *Journal of Nanoparticle Research* **2015**, *17* (3).
60. Paredes, J. I.; Villar-Rodil, S.; Martínez-Alonso, A.; Tascón, J. M. D., Graphene Oxide Dispersions in Organic Solvents. *Langmuir* **2008**, *24* (19), 10560-10564.

61. Bo, Z.; Shuai, X.; Mao, S.; Yang, H.; Qian, J.; Chen, J.; Yan, J., Green preparation of reduced graphene oxide for sensing and energy storage applications. *Scientific reports* **2014**.
62. Zhang, S.; Yang, J.; Chen, B. B.; Guo, S.; Li, J. F.; Li, C. S., One-step hydrothermal synthesis of reduced graphene oxide/zinc sulfide hybrids for enhanced tribological properties of epoxy coatings. *Surf Coat Tech* **2017**, *326*, 87-95.
63. Lyon, S. B.; Bingham, R.; Mills, D. J., Advances in corrosion protection by organic coatings: What we know and what we would like to know. *Progress in Organic Coatings* **2017**, *102*, 2-7.
64. Wang, D.; Bierwagen, G. R., Sol-gel coatings on metals for corrosion protection. *Progress in Organic Coatings* **2009**, *64* (4), 327-338.
65. Tetsuka, H.; Nagoya, A.; Asahi, R., Highly luminescent flexible amino-functionalized graphene quantum dots@ cellulose nanofiber-clay hybrids for white-light emitting diodes. *Journal of Materials Chemistry C* **2015**, *3* (15), 3536-3541.
66. Jeon, I. Y.; Shin, Y. R.; Sohn, G. J.; Choi, H. J.; Bae, S. Y.; Mahmood, J.; Jung, S. M.; Seo, J. M.; Kim, M. J.; Wook Chang, D.; Dai, L.; Baek, J. B., Edge-carboxylated graphene nanosheets via ball milling. *Proc Natl Acad Sci U S A* **2012**, *109* (15), 5588-93.
67. Dresselhaus, M. S.; Jorio, A.; Souza Filho, A. G.; Saito, R., Defect characterization in graphene and carbon nanotubes using Raman spectroscopy. *Philos Trans A Math Phys Eng Sci* **2010**, *368* (1932), 5355-77.
68. Dresselhaus, M. S.; Jorio, A.; Hofmann, M.; Dresselhaus, G.; Saito, R., Perspectives on carbon nanotubes and graphene Raman spectroscopy. *Nano Lett* **2010**, *10* (3), 751-8.
69. Dresselhaus, M. S.; Dresselhaus, G.; Hofmann, M., Raman spectroscopy as a probe of graphene and carbon nanotubes. *Philos Trans A Math Phys Eng Sci* **2008**, *366* (1863), 231-6.
70. Casiraghi, C.; Hartschuh, A.; Qian, H.; Piscanec, S.; Georgi, C.; Fasoli, A.; Novoselov, K. S.; Basko, D. M.; Ferrari, A. C., Raman spectroscopy of graphene edges. *Nano Lett* **2009**, *9* (4), 1433-41.
71. Cancado, L. G.; Takai, K.; Enoki, T.; Endo, M.; Kim, Y. A.; Mizusaki, H.; Jorio, A.; Coelho, L. N.; Magalhaes-Paniago, R.; Pimenta, M. A., General equation for the determination of the crystallite size L_a of nanographite by Raman spectroscopy. *Appl Phys Lett* **2006**, *88* (16).
72. Muzyka, R.; Drewniak, S.; Pustelny, T.; Chrubasik, M.; Gryglewicz, G., Characterization of Graphite Oxide and Reduced Graphene Oxide Obtained from Different Graphite Precursors and Oxidized by Different Methods Using Raman Spectroscopy. *Materials (Basel)* **2018**, *11* (7).
73. Zhao, Y. X.; Ding, H. L.; Zhong, Q., Preparation and characterization of aminated graphite oxide for CO₂ capture. *Applied Surface Science* **2012**, *258* (10), 4301-4307.

74. Dennis, R. V.; Patil, V.; Andrews, J. L.; Aldinger, J. P.; Yadav, G. D.; Banerjee, S., Hybrid nanostructured coatings for corrosion protection of base metals: a sustainability perspective. *Mater Res Express* **2015**, *2* (3).
75. Ramezanzadeh, B.; Ahmadi, A.; Mandavian, M., Enhancement of the corrosion protection performance and cathodic delamination resistance of epoxy coating through treatment of steel substrate by a novel nanometric sol-gel based silane composite film filled with functionalized graphene oxide nanosheets. *Corros Sci* **2016**, *109*, 182-205.
76. Corrosion Protection with Thinner Zinc Coating. *Ind Finish* **1975**, *51* (3), 56-57.
77. Feliu, S.; Morcillo, M.; Feliu, S., Deterioration of cathodic protection action of zinc-rich paint coatings in atmospheric exposure. *Corrosion-Us* **2001**, *57* (7), 591-597.
78. Shirehjini, F. T.; Danaee, I.; Eskandari, H.; Nikmanesh, S.; Zarei, D., Improvement of the sacrificial behavior of zinc in scratches of zinc-rich polymer coatings by incorporating clay nanosheets. *Mater Test* **2017**, *59* (7-8), 682-688.
79. Aponte, B.; de Romero, M. F.; de Rincon, O. T.; Arias, S.; Contreras, M.; Ramos, J.; Collantes, R., Corrosion costs in preventive and corrective maintenance in equipment and facilities in industry. *Rev Tec Fac Ing Univ* **2008**, *31*, 87-96.
80. Syrett, B. C.; Gorman, J. A.; Arey, M. L.; Koch, G. H.; Jacobson, G. A., Cost of corrosion - A recently completed study reveals the cost of corrosion in major sectors of the electric power industry. *Mater Performance* **2002**, *41* (3), 18-22.
81. Tuberquia, J. C.; Harl, R. R.; Jennings, G. K.; Rogers, B. R.; Bolotin, K. I., Graphene: Corrosion-Inhibiting Coating (vol 6, pg 1102, 2012). *Acs Nano* **2012**, *6* (5), 4540-4540.
82. Mousavinejad, T.; Bagherzadeh, M. R.; Akbarinezhad, E.; Ahmadi, M.; Guinel, M. J. F., A novel water-based epoxy coating using self-doped polyaniline-clay synthesized under supercritical CO₂ condition for the protection of carbon steel against corrosion. *Progress in Organic Coatings* **2015**, *79*, 90-97.
83. Ramezanzadeh, B.; Moghadam, M. H. M.; Shohani, N.; Mandavian, M., Effects of highly crystalline and conductive polyaniline/graphene oxide composites on the corrosion protection performance of a zinc-rich epoxy coating. *Chem Eng J* **2017**, *320*, 363-375.
84. Peplow, M., The quest for supercarbon. *Nature* **2013**.
85. Gong, P. W.; Wang, Z. F.; Fan, Z. J.; Hong, W.; Yang, Z. G.; Wang, J. Q.; Yang, S. R., Synthesis of chemically controllable and electrically tunable graphene films by simultaneously fluorinating and reducing graphene oxide. *Carbon* **2014**, *72*, 176-184.

86. Glover, C. F.; Richards, C.; Baker, J.; Williams, G.; McMurray, H. N., In-coating graphene nano-platelets for environmentally-friendly corrosion protection of iron. *Corros Sci* **2017**, *114*, 169-172.
87. Liu, D.; Zhao, W. J.; Liu, S.; Cen, Q. H.; Xue, Q. J., Comparative tribological and corrosion resistance properties of epoxy composite coatings reinforced with functionalized fullerene C60 and graphene. *Surf Coat Tech* **2016**, *286*, 354-364.
88. Huang, K. J.; Niu, D. J.; Liu, X.; Wu, Z. W.; Fan, Y.; Chang, Y. F.; Wu, Y. Y., Direct electrochemistry of catalase at amine-functionalized graphene/gold nanoparticles composite film for hydrogen peroxide sensor. *Electrochimica Acta* **2011**, *56* (7), 2947-2953.
89. Navaee, A.; Salimi, A., Efficient amine functionalization of graphene oxide through the Bucherer reaction: an extraordinary metal-free electrocatalyst for the oxygen reduction reaction. *RSC Advances* **2015**.
90. Al-Sammarraie, A. M. A.; Raheema, M. H., Electrodeposited Reduced Graphene Oxide Films on Stainless Steel, Copper, and Aluminum for Corrosion Protection Enhancement. *Int J Corros* **2017**.
91. Tetsuka, H.; Nagoya, A.; Asahi, R., Highly luminescent flexible amino-functionalized graphene quantum dots@cellulose nanofiber-clay hybrids for white-light emitting diodes. *Journal of Materials Chemistry C* **2015**, *3* (15), 3536-3541.
92. Ren, M.; Wang, X.; Dong, C.; Li, B.; Liu, Y.; Chen, T., Reduction and transformation of fluorinated graphene induced by ultraviolet irradiation. *Physical Chemistry ...* **2015**.
93. Wang, X.; Dai, Y.; Gao, J.; Huang, J.; Li, B.; Fan, C.; Yang, J.; Liu, X., High-yield production of highly fluorinated graphene by direct heating fluorination of graphene-oxide. *ACS Appl Mater Interfaces* **2013**, *5* (17), 8294-9.
94. Park, M. S.; Lee, Y. S., Functionalization of graphene oxide by fluorination and its characteristics. *J Fluorine Chem* **2016**, *182*, 91-97.
95. Shao, Y.; El-Kady, M. F.; Sun, J.; Li, Y.; Zhang, Q.; Zhu, M.; Wang, H.; Dunn, B.; Kaner, R. B., Design and Mechanisms of Asymmetric Supercapacitors. *Chem Rev* **2018**, *118* (18), 9233-9280.
96. Zhang, L. L.; Zhao, X. S., Carbon-based materials as supercapacitor electrodes. *Chemical Society Reviews* **2009**, *38* (9), 2520-2531.
97. Wang, Y. G.; Song, Y. F.; Xia, Y. Y., Electrochemical capacitors: mechanism, materials, systems, characterization and applications. *Chemical Society Reviews* **2016**, *45* (21), 5925-5950.

98. Wu, C.; Feng, F.; Xie, Y., Design of vanadium oxide structures with controllable electrical properties for energy applications. *Chem Soc Rev* **2013**, *42* (12), 5157-83.
99. Zhou, Y.; Guo, W.; Li, T., A review on transition metal nitrides as electrode materials for supercapacitors. *Ceramics International* **2019**, *45* (17), 21062-21076.
100. Anasori, B.; Gogotsi, Y., 2D Metal Carbides and Nitrides (MXenes) : Structure, Properties and Applications. Springer, Cham, 2019; pp. 1 online resource (xvii, 534 p. <http://dx.doi.org/10.1007/978-3-030-19026-2> MIT Access Only.
101. Jiang, Q.; Kurra, N.; Alhabeab, M.; Gogotsi, Y.; Alshareef, H. N., All Pseudocapacitive MXene-RuO₂ Asymmetric Supercapacitors. *Advanced Energy Materials* **2018**, *8* (13).
102. Jia, H.; Cai, Y.; Li, S.; Zheng, X.; Miao, L.; Wang, Z.; Qi, J.; Cao, J.; Feng, J.; Fei, W., In situ synthesis of core-shell vanadium nitride@N-doped carbon microsheet sponges as high-performance anode materials for solid-state supercapacitors. *J Colloid Interface Sci* **2020**, *560*, 122-129.
103. An, G.-H.; Lee, D.-Y.; Ahn, H.-J., Vanadium nitride encapsulated carbon fibre networks with furrowed porous surfaces for ultrafast asymmetric supercapacitors with robust cycle life. *Journal of Materials Chemistry A* **2017**, *5* (37), 19714-19720.
104. Choi, D.; Blomgren, G. E.; Kumta, P. N., Fast and Reversible Surface Redox Reaction in Nanocrystalline Vanadium Nitride Supercapacitors. *Adv Mater* **2006**, *18* (9), 1178-1182.
105. Bonso, J.; Rahy, A.; Perera, S.; Nour, N.; Seitz, O.; Chabal, Y.; Balkus, K.; Ferraris, J.; Yang, D., Exfoliated graphite nanoplatelets-V₂O₅ nanotube composite electrodes for supercapacitors. *Journal of Power Sources* **203**.
106. Perera, S. D.; Patel, B.; Bonso, J.; Grunewald, M.; Ferraris, J. P.; Balkus, K. J., Jr., Vanadium oxide nanotube spherical clusters prepared on carbon fabrics for energy storage applications. *ACS Appl Mater Interfaces* **2011**, *3* (11), 4512-7.
107. Kim, B.-H.; Kim, C. H.; Yang, K. S.; Rahy, A.; Yang, D. J., Electrospun vanadium pentoxide/carbon nanofiber composites for supercapacitor electrodes. *Electrochimica Acta* **2012**, *83*, 335-340.
108. Ran, F.; Wu, Y.; Jiang, M.; Tan, Y.; Liu, Y.; Kong, L.; Kang, L.; Chen, S., Nanocomposites based on hierarchical porous carbon fiber@vanadium nitride nanoparticles as supercapacitor electrodes. *Dalton Trans* **2018**, *47* (12), 4128-4138.
109. Zhou, X.; Shang, C.; Gu, L.; Dong, S.; Chen, X.; Han, P.; Li, L.; Yao, J.; Liu, Z.; Xu, H.; Zhu, Y.; Cui, G., Mesoporous coaxial titanium nitride-vanadium nitride fibers of core-shell structures for high-performance supercapacitors. *ACS Appl Mater Interfaces* **2011**, *3* (8), 3058-63.

110. Wu, Y.; Yang, Y.; Zhao, X.; Tan, Y.; Liu, Y.; Wang, Z.; Ran, F., A Novel Hierarchical Porous 3D Structured Vanadium Nitride/Carbon Membranes for High-performance Supercapacitor Negative Electrodes. *Nanomicro Lett* **2018**, *10* (4), 63.
111. Huang, J.; Peng, Z.; Xiao, Y.; Xu, Y.; Chen, L.; Xiong, Y.; Tan, L.; Yuan, K.; Chen, Y., Hierarchical Nanosheets/Walls Structured Carbon-Coated Porous Vanadium Nitride Anodes Enable Wide-Voltage-Window Aqueous Asymmetric Supercapacitors with High Energy Density. *Adv Sci (Weinh)* **2019**, *6* (16), 1900550.
112. Liu, T.; Tang, L.; Luo, H.; Cheng, S.; Liu, M., A promising water-in-salt electrolyte for aqueous based electrochemical energy storage cells with a wide potential window: highly concentrated HCOOK. *Chem Commun (Camb)* **2019**, *55* (85), 12817-12820.
113. Tomiyasu, H.; Shikata, H.; Takao, K.; Asanuma, N.; Taruta, S.; Park, Y. Y., An aqueous electrolyte of the widest potential window and its superior capability for capacitors. *Sci Rep* **2017**, *7*, 45048.
114. Han, J.; Zhang, H.; Varzi, A.; Passerini, S., Fluorine-Free Water-in-Salt Electrolyte for Green and Low-Cost Aqueous Sodium-Ion Batteries. *ChemSusChem* **2018**, *11* (21), 3704-3707.
115. Jiang, L.; Liu, L.; Yue, J.; Zhang, Q.; Zhou, A.; Borodin, O.; Suo, L.; Li, H.; Chen, L.; Xu, K.; Hu, Y. S., High-Voltage Aqueous Na-Ion Battery Enabled by Inert-Cation-Assisted Water-in-Salt Electrolyte. *Adv Mater* **2020**, *32* (2), e1904427.
116. Daraghmeh, A.; Hussain, S.; Saadeddin, I.; Servera, L.; Xuriguera, E.; Cornet, A.; Cirera, A., A Study of Carbon Nanofibers and Active Carbon as Symmetric Supercapacitor in Aqueous Electrolyte: A Comparative Study. *Nanoscale Res Lett* **2017**, *12* (1), 639.
117. Jiang, D. E.; Jin, Z.; Henderson, D.; Wu, J., Solvent Effect on the Pore-Size Dependence of an Organic Electrolyte Supercapacitor. *J Phys Chem Lett* **2012**, *3* (13), 1727-31.
118. Salunkhe, R. R.; Young, C.; Tang, J.; Takei, T.; Ide, Y.; Kobayashi, N.; Yamauchi, Y., A high-performance supercapacitor cell based on ZIF-8-derived nanoporous carbon using an organic electrolyte. *Chem Commun (Camb)* **2016**, *52* (26), 4764-7.
119. Zhong, C.; Deng, Y.; Hu, W.; Qiao, J.; Zhang, L.; Zhang, J., A review of electrolyte materials and compositions for electrochemical supercapacitors. *Chem Soc Rev* **2015**, *44* (21), 7484-539.
120. Van Aken, K. L.; Beidaghi, M.; Gogotsi, Y., Formulation of ionic-liquid electrolyte to expand the voltage window of supercapacitors. *Angew Chem Int Ed Engl* **2015**, *54* (16), 4806-9.
121. Yu, L.; Chen, G. Z., Ionic Liquid-Based Electrolytes for Supercapacitor and Supercapattery. *Front Chem* **2019**, *7*, 272.

122. Largeot, C.; Portet, C.; Chmiola, J.; Taberna, P. L.; Gogotsi, Y.; Simon, P., Relation between the ion size and pore size for an electric double-layer capacitor. *J Am Chem Soc* **2008**, *130* (9), 2730-1.
123. Bose, S.; Kuila, T.; Mishra, A. K.; Rajasekar, R.; Kim, N. H.; Lee, J. H., Carbon-based nanostructured materials and their composites as supercapacitor electrodes. *Journal of Materials Chemistry* **2012**, *22* (3), 767-784.
124. Simon, P.; Gogotsi, Y., Charge storage mechanism in nanoporous carbons and its consequence for electrical double layer capacitors. *Philos Trans A Math Phys Eng Sci* **2010**, *368* (1923), 3457-67.
125. Liu, M.; Su, B.; Tang, Y.; Jiang, X.; Yu, A., Recent Advances in Nanostructured Vanadium Oxides and Composites for Energy Conversion. *Advanced Energy Materials* **2017**, *7* (23).
126. Mendoza-Sanchez, B.; Gogotsi, Y., Synthesis of Two-Dimensional Materials for Capacitive Energy Storage. *Adv Mater* **2016**, *28* (29), 6104-35.
127. Bonso, J. S.; Rahy, A.; Perera, S. D.; Nour, N.; Seitz, O.; Chabal, Y. J.; Balkus, K. J.; Ferraris, J. P.; Yang, D. J., Exfoliated graphite nanoplatelets–V₂O₅ nanotube composite electrodes for supercapacitors. *Journal of Power Sources* **2012**, *203*, 227-232.
128. Liu, Y.; Wu, Q.; Liu, L.; Manasa, P.; Kang, L.; Ran, F., Vanadium nitride for aqueous supercapacitors: a topic review. *Journal of Materials Chemistry A* **2020**, *8* (17), 8218-8233.
129. Bondarchuk, O.; Morel, A.; Bélanger, D.; Goikolea, E.; Brousse, T.; Mysyk, R., Thin films of pure vanadium nitride: Evidence for anomalous non-faradaic capacitance. *Journal of Power Sources* **2016**, *324*, 439-446.
130. Yang, Y.; Shen, K.; Liu, Y.; Tan, Y.; Zhao, X.; Wu, J.; Niu, X.; Ran, F., Novel Hybrid Nanoparticles of Vanadium Nitride/Porous Carbon as an Anode Material for Symmetrical Supercapacitor. *Nanomicro Lett* **2017**, *9* (1), 6.
131. <Inner and Outer Active Surface of RuO₂ Electrodes.pdf>.
132. <High Perf V₂O₅ Pseudocaps Porous Nanowire Composites for Na-Ion.pdf>.
133. Brezesinski, K.; Wang, J.; Haetge, J.; Reitz, C.; Steinmueller, S. O.; Tolbert, S. H.; Smarsly, B. M.; Dunn, B.; Brezesinski, T., Pseudocapacitive contributions to charge storage in highly ordered mesoporous group V transition metal oxides with iso-oriented layered nanocrystalline domains. *J Am Chem Soc* **2010**, *132* (20), 6982-90.
134. <Dunn - Pseudocap Contribution of TiO₂ paper.pdf>.

BIOGRAPHICAL SKETCH

Melissa Ann Wunch was born in Naugatuck, CT, where she lived for seven years. She was raised in Cleveland, GA and attended primary through high school while living there. Upon graduation from White County High School, she then attended The Florida State University (FSU) where she received a BS degree in Biochemistry. During her time at FSU she competed on the intercollegiate bowling team, representing the university across the US in collegiate tournaments. After leaving FSU she moved on to attend graduate school and pursue her MS and PhD in Chemistry at The University of Texas at Dallas (UTD). Her research interest shifted from biochemistry to inorganic and materials chemistry. Currently she studies functionalized graphene materials for corrosion resistance and composite electrode materials for energy storage devices.

CURRICULUM VITAE

Melissa Ann Wunch

Department of Chemistry and Biochemistry

The University of Texas at Dallas

Richardson, TX, 75080

Executive Summary

Enthusiastic, hardworking, and self-driven researcher with 7 years of laboratory experience. Understanding of how to develop materials and methods which can be transitioned from lab scale to commercialization. Well experienced in the field of graphene functionalization and development of composite materials for corrosion resistance. Performed synthesis of transition metal oxides and worked on projects which composite them with carbon nanofibers for supercapacitor application. Experience in the synthesis of polyacrylonitrile (PAN) based polymers for carbon nanofibers and carbon fiber precursors using different monomers for cost reduction.

Education and Academic Experience

PhD in Chemistry, The University of Texas at Dallas

2017-2020

Advisor: Duck Joo Yang

Project: Preparation of functionalized graphenes and their performance for corrosion

Resistance

Synthesis of Vanadium nitride-carbon nanofiber mats and their application for asymmetric supercapacitor electrodes

MS in Chemistry, The University of Texas at Dallas

2014-2017

Advisor: Duck Joo Yang

Project: Functionalization and Dispersion Stability of Graphene Materials in 2K Urethane Coating System and Expanded interlayer spacing of vanadium oxide nanostructures for energy storage applications

BS in Biochemistry, The Florida State University

2007-2012

Advisor: Wei Yang

Project: Calculation of the free energy of a deprotonated Cysteine residue in solvent and aqueous environments using computational simulations

Presentations

- M. Wunch; S.F. Mahmood, D.J. Yang. Functionalized Graphene for Corrosion Protection in Two-Component Epoxy Coating, UKC National Conference (2019) August 14-17, Chicago, IL (oral)
- M. Wunch; S.F. Mahmood; D.J. Yang. Functionalization of Mechanically Exfoliated Graphene and its Mechanical and Dispersion Properties, UKC National Conference (2019) August 14-17, Chicago, IL (poster)
- M. Wunch; D.J. Yang. Functionalization and Dispersion Stability Study of Graphene Materials, UKC National Conference (2019) August 14-17, Chicago, IL (oral)
- M. Wunch; J.A. Garcia; S.F. Mahmood; K.J. Balkus Jr.; J.P. Ferraris; D.J. Yang, Vanadium Oxide Nanoflower-Carbon Nanofiber Composite Electrodes for Asymmetric Supercapacitors, 235th ECS Meeting and Exposition, 2019, May 26-31, Dallas, TX (oral)
- M. Wunch; S.F. Mahmood, D.J. Yang. Functionalization of Graphene for Corrosion Protection in Two-Component (2K) Urethane Coating, UKC National Conference (2018) August 1-4, Queens, NY (oral)
- M. Wunch; W. Perera; K.J. Balkus, Jr.; D.J. Yang. Low Temperature Synthesis of Amorphous Vanadium Pentoxide Nanofibers and their Transformation to Crystalline

Material, SERMACS-SWRM Regional Meeting, 2015, Memphis, TN, November 4-7
(poster)

- Choudhury, J. S. Bonso, M. Wunch, K. S. Yang, J. P. Ferraris, D. J. Yang, In-situ synthesis of vanadium pentoxide nanofibre/exfoliated graphene nanohybrid and its supercapacitor applications, SERMACS-SWRM Regional Meeting, 2015, Memphis, TN, November 4-7
(oral)

Publications

- M.Wunch; S.F. Mahmood; S.Lee; D.J.Yang, “Aminated and Fluorinated Graphene Based Coatings for Corrosion Resistance”, in submission *Corrosion Science*
- M.Wunch; B. Salazaar; S.Lee; D.J.Yang, “Green Synthesis of Aminated Mechanically Exfoliated Graphene”, in submission *RSC Advances*
- M.Wunch, S.F. Mahmood, D.J. Yang, “Facile direct functionalization of graphene nanoparticles”, *US Patent 20200087150 A1*, 2020
- A. Choudhury; D.N. Tran; M.Wunch; M.N. Nadagouda; R.S. Varma; and D.J. Yang, “Polyaniline: PANI nanofibers and nanotubes – Recent advances in the synthesis and their properties”, *CRC Concise Encyclopedia of Nanotech.*, **2016**, 923
- A.Choudhury; J.S. Bonso; M.Wunch; K.S. Yang; J.P. Ferraris; and D.J. Yang, “In-situ synthesis of vanadium pentoxide nanofiber/exfoliated graphene nanohybrid and its supercapacitor application”, *J. Power Sources*, 287, **2015**, 283-290.

Abstracts

- M. Wunch; S.F. Mahmood; D.J. Yang, Direct Functionalization of Graphene Nanoplatelets and their effect on Dispersion and Mechanical Properties, 259th ACS National Meeting and Exposition, Philadelphia, PA, March 22-26, 2020 (COLL 358/poster/SciMix)

- M. Wunch; J.A. Garcia; S.F. Mahmood; K.J. Balkus, Jr.; J.P. Ferraris; D.J. Yang, Vanadium Nitride – Carbon Nanofiber Composite Electrodes for Asymmetric Supercapacitors with Li-Doped Ionic Liquid Electrolyte, 259th ACS National Meeting and Exposition, Philadelphia, PA, March 22-26, 2020 (INOR 811/poster)
- M.Wunch; D.J. Yang, Facile and Direct Method of Amination of Mechanically Exfoliated Graphene, UKC National Conference, 2019, August 14-17, Chicago, IL
- M. Wunch; S.F. Mahmood; D.J. Yang, Functionalized Graphene for Corrosion Protection in Two-Component Epoxy Coating, UKC National Conference, 2019, August 14-17, Chicago, IL
- M. Wunch; J.A. Garcia; S.F. Mahmood; K.J. Balkus, Jr.; J.P. Ferraris; D.J. Yang, Vanadium Oxide Nanoflower-Carbon Nanofiber Composite Electrodes for Asymmetric Supercapacitors, 235th ECS Meeting and Exposition, 2019, May 26-31, Dallas, TX
- M.Wunch; W. Perera; K.J. Balkus, Jr.; D.J. Yang, Low Temperature Synthesis of Amorphous Vanadium Pentoxide Nanofibers and their Transformation to Crystalline Material, SERMACS-SWRM Regional Meeting, 2015, Memphis, TN, November 4-7 (poster)
- Choudhury, J. S. Bonso, M. Wunch, K. S. Yang, J. P. Ferraris, D. J. Yang, In-situ synthesis of vanadium pentoxide nanofibre/exfoliated graphene nanohybrid and its supercapacitor applications, SERMACS-SWRM Regional Meeting, 2015, Memphis, TN, November 4-7 (oral)

Professional Societies

Electrochemical Society

2019-Present

Korean-American Scientists and Engineers Association

2016-Present

American Chemical Society

2014-Present

Skills

- Knowledge of different instrumentation, development, research, and the analytical understanding required to work in a laboratory.
- Problem solving and organization
- Efficient communication and writing with the ability to communicate and collaborate well professionally